"Projections of oceanic N_2O emissions in the 21st century using the IPSL Earth System Model"

J. Martinez-Rey[1], L. Bopp[2], M. Gehlen[3], A. Tagliabue[4] and N. Gruber[5].

[1] Laboratoire des Sciences du Climat et de l'Environnement, IPSL, CEA/CNRS/UVSQ, Bat. 712 - Orme des Merisiers, F-91191 CE Saclay, Gif-sur-Yvette, France.
jorge.martinez-rey@lsce.ipsl.fr

[2] Laboratoire des Sciences du Climat et de l'Environnement, IPSL, CEA/CNRS/UVSQ, Bat. 712 - Orme des Merisiers, F-91191 CE Saclay, Gif-sur-Yvette, France.
laurent.bopp@lsce.ipsl.fr

[3] Laboratoire des Sciences du Climat et de l'Environnement, IPSL, CEA/CNRS/UVSQ, Bat. 712 - Orme des Merisiers, F-91191 CE Saclay, Gif-sur-Yvette, France.
marion.gehlen@lsce.ipsl.fr

[4] School of Environmental Sciences, University of Liverpool, 4 Brownlow Street, Liverpool L69 3GP, UK.
a.tagliabue@liverpool.ac.uk

[5] Environmental Physics, Institute of Biogeochemistry and Pollutant Dynamics, ETH, CHN E31.2, Universitaetstrasse 16, 8092 Zürich, Switzerland.
nicolas.gruber@env.ethz.ch

0. Abstract

The ocean is a substantial source of nitrous oxide (N_2O) to the atmosphere, but little is known on how this flux might change in the future. Here, we investigate the potential evolution of marine N_2O emissions in the 21st century in response to anthropogenic climate change using the global ocean biogeochemical model NEMO-PISCES. Assuming nitrification as the dominant N_2O formation pathway, we implemented two different parameterizations of N_2O production which differ primarily at low oxygen (O_2) conditions. When forced with output from a climate model simulation run under the business-as-usual high CO_2 concentration scenario (RCP8.5), our simulations suggest a decrease of 4 to 12 % in N_2O emissions from 2005 to 2100, i.e., a reduction from 4.03 / 3.71 to 3.54 / 3.56 TgN yr^{-1} depending on the parameterization. The emissions decrease strongly in the western basins of the Pacific and Atlantic oceans, while they tend to increase above the Oxygen Minimum Zones (OMZs), i.e., in the Eastern Tropical Pacific and in the northern Indian Ocean. The reduction in N_2O emissions is caused on the one hand by weakened nitrification as a consequence of reduced primary and export production, and on the other hand by stronger vertical stratification, which reduces the transport of N_2O from the ocean interior to the ocean surface. The higher emissions over the OMZ are linked to an expansion of these zones under global warming, which leads to increased N_2O production associated primarily with denitrification. While there are many uncertainties in the relative contribution and changes in the N_2O production pathways, the increasing storage seems unequivocal and determines largely the decrease in N_2O emissions in the future. From the perspective of a global climate system, the averaged feedback strength associated with the projected decrease in oceanic N_2O emissions amounts to around -0.009 W m^{-2}K^{-1}, which is comparable to the potential increase from terrestrial N_2O sources. However, the assesment for a compensation between the terrestrial and marine feedbacks calls for an improved representation of N_2O production terms in fully coupled next generation of Earth System Models.

54 1 Introduction
55
56 Nitrous oxide (N_2O) is a gaseous compound responsible for two key feedback
57 mechanisms within the Earth's climate. First, it acts as a long-lived and powerful
58 greenhouse gas (Prather et al., 2012) ranking third in anthropogenic radiative forcing
59 after carbon dioxide (CO_2) and methane (CH_4) (Myrhe et al., 2013). Secondly, the
60 ozone (O_3) layer depletion in the future might be driven mostly by N_2O after the drastic
61 reductions in CFCs emissions start to show their effect on stratospheric chlorine levels
62 (Ravishankara et al., 2009). The atmospheric concentration of N_2O is determined by the
63 natural balance between sources from land and ocean and the destruction of N_2O in the
64 atmosphere largely by photolysis (Crutzen, 1970; Johnston, 1971). The natural sources
65 from land and ocean amount to ~6.6 and 3.8 TgN yr^{-1}, respectively (Ciais et al., 2013).
66 Anthropogenic activities currently add an additional 6.7 TgN yr^{-1} to the atmosphere,
67 which has caused atmospheric N_2O to increase by 18% since pre-industrial times (Ciais
68 et al., 2013), reaching 325 ppb in the year 2012 (NOAA ESRL Global Monitoring
69 Division, Boulder, Colorado, USA, http://esrl.noaa.gov/gmd/).
70 Using a compilation of 60,000 surface ocean observations of the partial pressure of N_2O
71 (pN_2O), Nevison et al. (2004) computed a global ocean source of 4 TgN yr^{-1}, with a
72 large range of uncertainty from 1.2 to 6.8 TgN yr^{-1}. Model derived estimates also differ
73 widely, i.e., between 1.7 and 8 TgN yr^{-1} (Nevison et al., 2003; Suntharalingam et al.,
74 2000). These large uncertainties are a consequence of too few observations and of poorly
75 known N_2O formation mechanisms, reflecting a general lack of understanding of key
76 elements of the oceanic nitrogen cycle (Gruber and Galloway, 2008; Zehr and Ward,
77 2002), and of N_2O in particular (e.g., Zamora et al., 2012, Bange et al., 2009 or Freing
78 et al., 2012, among others). A limited number of interior ocean N_2O observations were
79 made available only recently (Bange et al., 2009), but they contain large temporal and
80 spatial gaps. Information on the rates of many important processes remains insufficient,
81 particularly in natural settings. There are only few studies from a limited number of
82 specific regions such as the Arabian Sea, Central and North Pacific, Black Sea, the
83 Bedford Basin and the Scheldt estuary, which can be used to derive and test model
84 parameterisations (Mantoura et al., 1993; Bange et al., 2000; Elkins et al., 1978; Farias et
85 al., 2007; Frame and Casciotti, 2010; Westley et al., 2006; Yoshida et al., 1989; Punshon

86 and Moore, 2004; De Wilde and De Bie, 2000).
87 N_2O is formed in the ocean interior through two major pathways and consumed only in
88 oxygen minimum zones through denitrification (Zamora et al., 2012). The first
89 production pathway is associated with nitrification (conversion of ammonia, NH_4^+, into
90 nitrate, NO_3^-), and occurs when dissolved O_2 concentrations are above 20 µmol L^{-1}. We
91 subsequently refer to this pathway as the high-O_2 pathway. The second production
92 pathway is associated with a series of processes when O_2 concentrations fall below ~5
93 µmol L^{-1} and involve a combination of nitrification and denitrification (hereinafter
94 referred to as low-O_2 pathway) (Cohen and Gordon, 1978; Goreau et al., 1980; Elkins et
95 al., 1978). As nitrification is one of the processes involved in the aerobic remineralization
96 of organic matter, it occurs nearly everywhere in the global ocean with a global rate at
97 least one order of magnitude larger than the global rate of water column denitrification
98 (Gruber, 2008). A main reason is that denitrification in the water column is limited to
99 the OMZs, which occupy only a few percent of the total ocean volume (Bianchi et al.,
100 2012). This is also the only place in the water column where N_2O is being consumed.
101 The two production pathways have very different N_2O yields, i.e., fractions of nitrogen-
102 bearing products that are transformed to N_2O. For the high-O_2 pathway, the yield is
103 typically rather low, i.e., only about 1 in several hundred molecules of ammonium
104 escapes as N_2O (Cohen and Gordon, 1979). In contrast, in the low-O_2 pathway, and
105 particularly during denitrification, this fraction may go up to as high as 1:1, i.e., that all
106 nitrate is turned into N_2O (Tiedje, 1988). The relative contribution of the two pathways
107 to global N_2O production is not well established. Sarmiento and Gruber (2006)
108 suggested that the two may be of equal importance, but more recent estimates suggest
109 that the high-O_2 production pathway dominates global oceanic N_2O production (Freing
110 et al., 2012).
111 Two strategies have been pursued in the development of parameterizations for N_2O
112 production in global biogeochemical models. The first approach builds on the
113 importance of the nitrification pathway and its close association with the aerobic
114 remineralization of organic matter. As a result the production of N_2O and the
115 consumption of O_2 are closely tied to each other, leading to a strong correlation between
116 the concentration of N_2O and the apparent oxygen utilization (AOU). This has led to the
117 development of two sets of parameterizations, one based on concentrations, i.e., directly

as a function of AOU (Butler et al., 1989) and the other based on the rate of oxygen utilization, i.e. OUR (Freing et al., 2009). Additional variables have been introduced to allow for differences in the yield, i.e., the ratio of N_2O produced over oxygen consumed, such as temperature (Butler et al., 1989) or depth (Freing et al., 2009). In the second approach, the formation of N_2O is modeled more mechanistically, and tied to both nitrification and denitrification by an O_2 dependent yield (Suntharalingam and Sarmiento, 2000; Nevison et al., 2003; Jin and Gruber, 2003). Since most models do not include nitrification explicitly, the formation rate is actually coupled directly to the remineralization of organic matter. Regardless of the employed strategy, all parameterizations depend to first order on the amount of organic matter that is being remineralized in the ocean interior, which is governed by the export of organic carbon to depth. The dependence of N_2O production on oxygen levels and on other parameters such as temperature only acts at second order. This has important implications not only for the modeling of the present-day distribution of N_2O in the ocean, but also for the sensitivity of marine N_2O to future climate change.

Over this century, climate change will perturb marine N_2O formation in multiple ways. Changes in productivity will drive changes in the export of organic matter to the ocean interior (Steinacher et al., 2010; Bopp et al., 2013) and hence affect the level of marine nitrification. Ocean warming might change the rate of N_2O production during nitrification (Freing et al., 2012). Changes in carbonate chemistry (Bindoff et al., 2007) might cause changes in the C:N ratio of the exported organic matter (Riebesell et al., 2007), altering not only the rates of nitrification, but also the ocean interior oxygen levels (Gehlen et al., 2011). Finally, the expected general loss of oxygen (Keeling et al., 2010; Cocco et al., 2012; Bopp et al., 2013) could substantially affect N_2O production via both nitrifier denitrification and classic denitrification.

Ocean biogeochemical models used for IPCC's 4^{th} assessment report estimated a decrease between 2% and 13% in primary production (PP) under the business-as-usual high CO_2 concentration scenario A2 (Steinacher et al., 2010). A more recent multi-model analysis based on the models used in IPCC's 5^{th} assessment report also suggest a large reduction of PP down to 18% by 2100 for the RCP8.5 scenario (Bopp et al., 2013). In these simulations, the export of organic matter is projected to decrease between 6% and 18% in 2100 (Bopp et al., 2013), with a spatially distinct pattern: in general, productivity and

export are projected to decrease at mid- to low-latitudes in all basins, while productivity and export are projected to increase in the high-latitudes and in the South Pacific subtropical gyre (Bopp et al., 2013). A wider spectrum of responses was reported regarding changes in the ocean oxygen content. While all models simulate decreased oxygen concentrations in response to anthropogenic climate change (by about 2 to 4% in 2100), and particularly in the mid-latitude thermocline regions, no agreement exists with regard to the hypoxic regions, i.e., those having oxygen levels below 60 µmol L^{-1} (Cocco et al., 2012; Bopp et al., 2013). Some models project these regions to expand, while others project a contraction. Even more divergence in the results exists for the suboxic regions, i.e., those having O_2 concentrations below 5 µmol L^{-1} (Keeling et al., 2010; Deutsch et al., 2011; Cocco et al., 2012; Bopp et al., 2013), although the trend for most models is pointing towards an expansion. At the same time, practically none of the models is able to correctly simulate the current distribution of oxygen in the OMZ (Bopp et al., 2013). In summary, while it is clear that major changes in ocean biogeochemistry are looming ahead (Gruber, 2011), with substantial impacts on the production and emission of N_2O, our ability to project these changes with confidence is limited.

In this study, we explore the implications of these future changes in ocean physics and biogeochemistry on the marine N_2O cycle, and make projections of the oceanic N_2O emissions from year 2005 to 2100 under the high CO_2 concentration scenario RCP8.5. We analyze how changes in biogeochemical and physical processes such as net primary production (NPP), export production and vertical stratification in this century translate into changes in oceanic N_2O emissions to the atmosphere. To this end, we use the NEMO-PISCES ocean biogeochemical model, which we have augmented with two different N_2O parameterizations, permitting us to evaluate changes in the marine N_2O cycle at the process level, especially with regard to production pathways in high and low oxygen regimes. We demonstrate that while future changes in the marine N_2O cycle will be substantial, the net emissions of N_2O appear to change relatively little, i.e., they are projected to decrease by about 10% in 2100.

2. Methodology

2.1 NEMO-PISCES Model

Future projections of the changes in the oceanic N_2O cycle were performed using the PISCES ocean biogeochemical model (Aumont and Bopp, 2006) in offline mode with physical forcings derived from the IPSL-CM5A-LR coupled model (Dufresne et al., 2013). The horizontal resolution of NEMO ocean general circulation model is 2° x 2° cos Ø (Ø being the latitude) with enhanced latitudinal resolution at the equator of 0.5°. PISCES is a biogeochemical model with five nutrients (NO_3, NH_4, PO_4, Si and Fe), two phytoplankton groups (diatoms and nanophytoplankton), two zooplankton groups (micro and mesozooplankton), and two non-living compartments (particulate and dissolved organic matter). Phytoplankton growth is limited by nutrient availability and light. Constant Redfield C:N:P ratios of 122:16:1 are assumed (Takahashi et al., 1985), while all other ratios, i.e., those associated with chlorophyll, iron, and silicon (Chl:C, Fe:C and Si:C) vary dynamically.

2.2 N_2O parameterizations in PISCES

We implemented two different parameterizations of N_2O production in NEMO-PISCES. The first one, adapted from Butler et al. (1989) follows the oxygen consumption approach, with a temperature dependent modification of the N_2O yield (P.TEMP). The second one is based on Jin and Gruber (2003) (P.OMZ), following the more mechanistic approach, i.e., it considers the different processes occurring at differing oxygen concentrations in a more explicit manner.

The P.TEMP parameterization assumes that the N_2O production is tied to nitrification only with a yield that is at first order constant. This is implemented in the model by tying the N_2O formation in a linear manner to O_2 consumption. A small temperature dependence is added to the yield to reflect the potential impact of temperature on metabolic rates. The production term of N_2O, i.e., $J^{P.TEMP}(N_2O)$, is then mathematically formulated as:

$$J^{P.TEMP}(N_2O) = (\gamma + \theta\, T\,)\, J(O_2)_{consumption} \quad (1)$$

where γ is a background yield (0.53 x 10^{-4} mol N_2O/mol O_2 consumed), θ is the temperature dependency of γ (4.6 x 10^{-6} mol N_2O (mol O_2)$^{-1}$ K^{-1}), T is temperature (K),

and $J(O_2)_{consumption}$ is the sum of all biological O_2 consumption terms within the model. The same ratio between constants γ and θ is used in the model as in the original formulation from Butler et al. (1989). Although this parameterization is very simple, a recent analysis of N_2O observations supports such an essentially constant yield, even in the OMZ of the Eastern Tropical Pacific (Zamora et al., 2012).

The P.OMZ parameterization, formulated after Jin and Gruber (2003), assumes that the overall yield consists of a constant background yield and an oxygen dependent yield. The former is presumed to represent the N_2O production by nitrification, while the latter is presumed to reflect the enhanced production of N_2O at low oxygen concentrations, in part driven by denitrification, but possibly including nitrification as well. This parameterization includes the consumption of N_2O in suboxic conditions. This gives:

$$J^{P.OMZ}(N_2O) = (\alpha + \beta f(O_2))J(O_2)_{consumption} - k\,N_2O \quad (2)$$

where α is, as in Eq.(1), a background yield ($0.9 \cdot 10^{-4}$ mol N_2O/mol O_2 consumed), β is a yield parameter that scales the oxygen dependent function ($6.2 \cdot 10^{-4}$), $f(O_2)$ is a unitless oxygen-dependent step-like modulating function, as suggested by laboratory experiments (Goreau et al., 1980) (Fig. S1, Supplementary Material), and k is the 1st order rate constant of N_2O consumption close to anoxia (zero otherwise). For k, we have adopted a value of 0.138 yr^{-1} following Bianchi et al. (2012) while we set the consumption regime for O_2 concentrations below 5 µmol L^{-1}. The constant α is in the same order of magnitude as the one proposed by Jin and Gruber (2003), while β is two orders of magnitude smaller. The use of the original value would result in a significant increase of N_2O production associated with OMZs and, hence, in a departure from the assumption of dominant nitrification.

The P.OMZ parameterization permits us the independent quantification of the N_2O formation pathways associated with nitrification and those associated with low-oxygen concentrations (nitrification/denitrification) and their evolution in time over the next century. Specifically, we consider the source term $\alpha\, J(O_2)_{consumption}$ as that associated with the nitrification pathway, while we associated the source term $\beta f(O_2)\, J(O_2)_{consumption}$ with the low-oxygen processes (Fig. S2, Supplementary Material).

N_2O production is inhibited by light in the model, and therefore N_2O production in P.TEMP and P.OMZ parameterizations only occurs below a fixed depth of 100m.

We employ a standard bulk approach for simulating the loss of N_2O to the atmosphere via gas exchange. We use the formulation of Wanninkhof et al. (1992) for estimating the gas transfer velocity, adjusting the Schmidt number for N_2O and using the solubility constants of N_2O given by Weiss and Price (1980). We assume a constant atmospheric N_2O concentration of 284 ppb in all simulations to explore future changes inherent to ocean processes without feedbacks due to changes in the atmosphere.

2.3 Experimental design

NEMO-PISCES was first spun up during 3000 years using constant pre-industrial dynamical forcings fields from IPSL-CM5A-LR (Dufresne et al., 2013) without activating the N_2O parameterizations. This spin-up phase was followed by a 150-yr long simulation, forced by the same dynamical fields now with N_2O production and N_2O sea-to-air flux embedded. The N_2O concentration at all grid points was prescribed initially to 20 nmol L^{-1}, which is consistent with the MEMENTO database average value of 18 nmol L^{-1} below 1500m (Bange et al., 2009). During the 150-yr spin-up, we diagnosed the total N_2O production and N_2O sea-to-air flux and adjusted the α, β, γ and θ parameters in order to achieve a total N_2O sea-to-air flux in the two parameterizations at equilibrium close to 3.85 TgN yr^{-1} (Ciais et al., 2013). In addition, the relative contribution of the high-O_2 pathway in the P.OMZ parameterization was set to 75% of the total N_2O production based on Suntharalingam et al. (2000), where a sensitivity model analysis on the relative contribution of high- and low-O_2 production pathways showed that a higher contribution of nitrification (75%) than denitrification (25%) achieved the best model performance compared to the data product from Nevison et al. (1995). P.TEMP can be considered as 100% nitrification, testing in this way the hypothesis of nitrification as the dominant pathway of N_2O production on a global scale. Nitrification could contribute with up to 93% of the total production based on estimations considering N_2O production along with water mass transport (Freing et al., 2012).

Projections in NEMO-PISCES of historical (from 1851 to 2005) and future (from 2005 to 2100) simulated periods were done using dynamical forcing fields from IPSL-CM5A-LR. These dynamical forcings were applied in an offline mode, i.e. monthly means of

276 temperature, velocity, wind speed or radiative flux were used to force NEMO-PISCES.
277 Future simulations used the business-as-usual high CO_2 concentration scenario (RCP8.5)
278 until year 2100. Century scale model drifts for all the biogeochemical variables presented,
279 including N_2O sea-to-air flux, production and inventory, were removed using an
280 additional control simulation with IPSL-CM5A-LR pre-industrial dynamical forcing
281 fields from year 1851 to 2100. Despite the fact that primary production and the export
282 of organic matter to depth were stable in the control simulation, the air-sea N_2O
283 emissions drifted (an increase of 5 to 12% in 200 yr depending on the parameterization)
284 due to the short spin-up phase (150 yrs) and to the choice of the initial conditions for
285 N_2O concentrations.
286
287 3. Present-day oceanic N_2O
288
289 3.1 Contemporary N_2O fluxes
290
291 The model simulated air-sea N_2O emissions show large spatial contrasts, with flux
292 densities varying by one order of magnitude, but with relatively small differences between
293 the two parameterizations (Fig. 1a and 1b). This is largely caused by our assumption that
294 the dominant contribution (75%) to the total N_2O production in the P.OMZ
295 parameterization is the nitrification pathway, which is then not so different from the
296 P.TEMP parameterization, where it is 100%. As a result, the major part of N_2O is
297 produced in the subsurface via nitrification, contributing directly to imprint changes into
298 the sea-to-air N_2O flux without a significant meridional transport (Suntharalingam and
299 Sarmiento, 2000).
300 Elevated N_2O emission regions (> 50 mgN m^{-2} yr^{-1}) are found in the Equatorial and
301 Eastern Tropical Pacific, in the northern Indian ocean, in the northwestern Pacific, in the
302 North Atlantic and in the Agulhas Current. In contrast, low fluxes (< 10 mgN m^{-2} yr^{-1})
303 are simulated in the Southern Ocean, Atlantic and Pacific subtropical gyres and southern
304 Indian Ocean. The large scale distribution of N_2O fluxes is coherent with Nevison et al.
305 (2004) (Fig. 1c). This comes as a natural consequence of the relatively high contribution
306 of nitrification and hence hotspots of N_2O emissions are associated with regions where
307 higher export of organic matter occurs in the model.

There are however several discrepancies between the model and the data product. At high latitudes, the high N_2O emissions observed in the North Pacific are not well represented in our model, with a significant shift towards the western part of the Pacific basin, similar to other modeling studies (e.g., Goldstein et al., 2003; Jin and Gruber, 2003). The OMZ in the North Pacific, located at approximately 600m deep, is underestimated in the model due to the deficient representation of the Meridional Overturning Circulation (MOC) in the North Pacific in global ocean biogeochemical models, which in turn might suppress low oxygenated areas and therefore one potential N_2O source. Discrepancies between model and observations also occur in the Southern Ocean, a region whose role in global N_2O fluxes remains debated due to the lack of observations and the occurrence of potential artifacts due to interpolation techniques reflected in data products such as that from Nevison et al., 2004. (e.g., Suntharalingam and Sarmiento, 2000, and Nevison et al, 2003). The model also overestimates N_2O emissions in the North Atlantic. The emphasis put on the nitrification pathway suggests that hotspots of carbon export are at the origin of elevated concentrations of N_2O in the subsurface. N_2O is quickly outgassed to the atmosphere, leading to such areas of high N_2O emissions in the model.

Model-data discrepancies can be seen as a function of latitude in Figure 1d. The modeled N_2O flux maxima peak at around 40°S, i.e., around 10° north to that estimated by Nevison et al. (2004), although Southern Ocean data must be interpreted with caution. In the northern hemisphere the stripe in the North Pacific in not captured by the model, splitting the flux from the 45°N band into two peaks at 38°N and 55°N

3.2 Contemporary N_2O concentrations and the relationship to O_2

The model results at present day were evaluated against the MEMENTO database (Bange et al., 2009), which contains about 25,000 measurements of co-located N_2O and dissolved O_2 concentrations. Table 1 summarizes the standard deviation and correlation coefficients for P.TEMP and P.OMZ compared to MEMENTO. The standard deviation of the model output is very similar to MEMENTO, i.e., around 16 nmol L^{-1} of N_2O. However, the correlation coefficients between the sampled data points from MEMENTO and P.TEMP / P.OMZ are 0.49 and 0.42 respectively. Largest

340 discrepancies are found mostly in the deep ocean and in the OMZs.
341 Figure 2 compares the global average vertical profile of the observed N_2O against the
342 results from the two parameterisations. The in-situ observations show three characteristic
343 layers: the upper 100m layer with low (~10 nmol L^{-1}) N_2O concentration due to gas
344 exchange keeping N_2O close to its saturation concentration, the mesopelagic layer,
345 between 100 and 1500m, where N_2O is enriched via nitrification and denitrification in
346 the OMZs, and the deep ocean beyond 1500m, with a relatively constant concentration
347 of 18 nmol L^{-1} on average. Both parameterizations underestimate the N_2O concentration
348 in the upper 100 meters, where most of the N_2O is potentially outgassed to the
349 atmosphere. In the second layer, P.OMZ shows a fairly good agreement with the
350 observations in the 500 to 900m band, whereas P.TEMP is too low by ~10 nmol L^{-1}.
351 Below 1500m, both parameterizations simulate too high N_2O compared to the
352 observations. This may be caused by the lack or underestimation of a sink process in the
353 deep ocean, or by the too high concentrations used to intialize the model, which persist
354 due to the rather short spin-up time of only 150 yrs.
355 The analysis of the model simulated N_2O concentrations as a function of model
356 simulated O_2 shows the differences between the two parameterizations more clearly (Fig.
357 3a and 3b). Such a plot allows us to assess the model performance with regard to N_2O
358 (Jin and Gruber, 2003), without being subject to the strong potential biases introduced
359 by the model's deficiencies in simulating the distribution of O_2. This is particularly
360 critical in the OMZs, where all models exhibit strong biases (Cocco et al., 2012; Bopp et
361 al., 2013) (see also Fig. 3c). P.TEMP (Fig. 3a) slightly overestimates N_2O for dissolved
362 O_2 concentrations above 100 µmol L^{-1}, and does not fully reproduce either the high N_2O
363 values in the OMZs or the N_2O depletion when O_2 is almost completely consumed.
364 P.OMZ (Figure 3b) overestimates the N_2O concentration over the whole range of O_2,
365 with particularly high values of N_2O above 100 nmol L^{-1} due to the exponential function
366 used in the OMZs. There, the observations suggest concentrations below 80 nmol L^{-1} for
367 the same low O_2 values, consistent with the linear trend observed for higher O_2, which
368 seems to govern over most of the O_2 spectrum, as suggested by Zamora et al. (2012). The
369 discrepancy at low O_2 concentration may also stem from our choice of a too low N_2O
370 consumption rate under essentially anoxic conditions. Finally, it should be considered
371 that most of the MEMENTO data points are from OMZs and therefore N_2O

372 measurements could be biased towards higher values than the actual open ocean average,
373 where our model performs better.
374
375 4. Future oceanic N_2O
376
377 4.1 N_2O sea-to-air flux
378
379 The global oceanic N_2O emissions decrease relatively little over the next century (Fig. 4a)
380 between 4% and 12%. Namely, in P.TEMP, the emissions decrease by 0.15 TgN yr^{-1}
381 from 3.71 TgN yr^{-1} in 1985-2005 to 3.56 TgN yr^{-1} in 2080-2100 and in P.OMZ, the
382 decrease is slightly larger at 12%, i.e., amounting to 0.49 Tg N yr^{-1} from 4.03 to 3.54
383 TgN yr^{-1}. Notable is also the presence of a negative trend in N_2O emissions over the 20^{th}
384 century, most pronounced in the P.OMZ parameterization. Considering the change over
385 the 20^{th} and 21^{st} centuries together, the decreases increase to 7 and 15%.
386 These relatively small global decreases mask more substantial changes at the regional scale,
387 with a mosaic of regions experiencing a substantial increase and regions experiencing a
388 substantial decrease (Fig. 4b and 4c). In both parameterizations, the oceanic N_2O
389 emissions decrease in the northern and south western oceanic basins (e.g., the North
390 Atlantic and Arabian Sea), by up to 25 mgN $m^{-2}yr^{-1}$. In contrast, the fluxes are simulated
391 to increase in the Eastern Tropical Pacific and in the Bay of Bengal. For the Benguela
392 Upwelling System (BUS) and the North Atlantic a bi-modal pattern emerges in 2100. As
393 was the case for the present-day distribution of the N_2O fluxes, the overall similarity
394 between the two parameterizations is a consequence of the dominance of the nitrification
395 (high-O_2) pathway in both parameterizations.
396 Nevertheless there are two regions where more substantial differences between the two
397 parameterizations emerge: the region overlying the oceanic OMZ at the BUS and the
398 Southern Ocean. In particular, the P.TEMP parameterization projects a larger
399 enhancement of the flux than P.OMZ at the BUS, whereas the emissions in the Southern
400 Ocean are enhanced in the P.OMZ parameterization.
401
402 4.2 Drivers of changes in N_2O emissions
403

The changes in N_2O emissions may stem from a change in net N_2O production, a change in the transport of N_2O from its location of production to the surface, or any combination of the two, which includes also changes in N_2O storage. Next we determine the contribution of these mechanisms to the overall decrease in N_2O emissions that our model simulated for the 21st century.

4.2.1 Changes in N_2O production

In both parameterizations, global N_2O production is simulated to decrease over the 21st century. The total N_2O production in P.OMZ decreases by 0.41 TgN yr^{-1} in 2080-2100 compared to the mean value over 1985-2005 (Fig. 5a). The parameterization P.OMZ allows to isolate the contributions of high- and low-O_2 and will be analysed in greater detail in the following sections. N_2O production via the high-O_2 pathway in P.OMZ decreases in the same order than total production, by 0.35 TgN yr^{-1} in 2080-2100 compared to present. The N_2O production in the low-O_2 regions remains almost constant across the experiment. In P.TEMP parameterization, the reduction in N_2O production is much weaker than in P.OMZ due to the effect of the increasing temperature. N_2O production decreases by 0.07 TgN yr^{-1} in 2080-2100 compared to present (Fig. 5b).

The vast majority of the changes in the N_2O production in the P.OMZ parameterization is caused by the high-O_2 pathway with virtually no contribution from the low-O_2 pathway (Fig. 5a). As the N_2O production in P.OMZ parameterization is solely driven by changes in the O_2 consumption (Eq. (2)), which in our model is directly linked to export production, the dominance of this pathway implies that primary driver for the future changes in N_2O production in our model is the decrease in export of organic matter (CEX). It was simulated to decrease by 0.97 PgC yr^{-1} in 2100, and the high degree of correspondence in the temporal evolution of export and N_2O production in Fig. 5a confirms this conclusion.

The close connection between N_2O production associated with the high-O_2 pathway and changes in export production is also seen spatially (Fig. 5c), where the spatial pattern of changes in export and changes in N_2O production are extremely highly correlated (shown by stippling). Most of the small deviations are caused by lateral advection of organic

carbon, causing a spatial separation between changes in O_2 consumption and changes in organic matter export.

As there is an almost ubiquitous decrease of export in all of the major oceanic basins except at high latitudes, N_2O production decreases overall as well. Hotspots of reductions exceeding -10 mgN $m^{-2}yr^{-1}$ are found in the North Atlantic, the western Pacific and Indian basins (Fig. 5c). The fewer places where export increases, are also the locations of enhanced N_2O production. For example, a moderate increase of 3 mgN m^{-2} yr^{-1} is projected in the Southern Ocean, South Atlantic and Eastern Tropical Pacific. The general pattern of export changes, i.e., decreases in lower latitudes, increase in higher latitudes, is consistent generally with other model projection patterns (Bopp et al., 2013), although there exist very strong model-to-model differences at the more regional scale.

Although the global contribution of the changes in the low-O_2 N_2O production is small, this is the result of regionally compensating trends. In the model's OMZs, i.e., in the Eastern Tropical Pacific and in the Bay of Bengal, a significant increase in N_2O production is simulated in these locations (Fig. 5d), with an increase of more than 15 mgN m^{-2} yr^{-1}. This increase is primarily driven by the expansion of the OMZs in our model (shown by stippling), while changes in export contribute less. In effect, NEMO-PISCES projects a 20% increase in the hypoxic volume globally, from 10.2 to 12.3 x 10^6 km^3, and an increase in the suboxic volume from 1.1 to 1.6 x 10^6 km^3 in 2100 (Fig. 5e). Elsewhere, the changes in the N_2O production through the low-O_2 pathway are dominated by the changes in export, thus following the pattern of the changes seen in the high-O_2 pathway. Overall these changes are negative, and happen to nearly completely compensate the increase in production in the OMZs, resulting in the near constant global N_2O production by the low-O_2 production pathway up to year 2100.

4.2.2 Changes in storage of N_2O

A steady increase in the N_2O inventory is observed from present to 2100. The pool of oceanic N_2O down to 1500m, i.e., potentially outgassed to the atmosphere, increases by 8.9 TgN from 1985-2005 to year 2100 in P.OMZ, whereas P.TEMP is less sensitive to changes with an increase of 4.0 TgN on the time period considered (Fig. 6a). The inventory in the upper 1500m in P.OMZ is 237.0 TgN at present, while in P.TEMP in

468 the same depth band is 179.8 TgN. This means that the projected changes in the
469 inventory represent an increase of about 4% and 2% in P.OMZ and P.TEMP
470 respectively.
471 This increase in storage of N_2O in the ocean interior shows an homogeneous pattern for
472 P.TEMP, with particular hotspots in the North Pacific, North Atlantic and the eastern
473 boundary currents in the Pacific (Fig. 6b). The spatial variability is more pronounced in
474 P.OMZ (Fig. 6c), related in part to the enhanced production associated with OMZs.
475 Most of the projected changes in storage are associated with shoaling of the mixed layer
476 depth (shown by stippling), suggesting that increase in N_2O inventories is caused by
477 increased ocean stratification. Enhanced ocean stratification, in turn, occurs in response
478 to increasing sea surface temperatures associated with global warming (Sarmiento et al.,
479 2004).
480
481 4.2.3 Effects of the combined mechanisms on N_2O emissions
482
483 The drivers of the future evolution of oceanic N_2O emissions emerge from the preceding
484 analysis. Firstly, a decrease in the high-O_2 production pathway driven by a reduced
485 organic matter remineralization reduces N_2O concentrations below the euphotic zone.
486 Secondly, the increased N_2O inventory at depth is caused by increased stratification and
487 therefore to a less efficient transport to the sea-to-air interface, leading to a less N_2O flux.
488 The global changes in N_2O flux, N_2O production and N_2O storage for P.OMZ are
489 presented in Fig. 7. Changes in N_2O flux and N_2O production are mostly of the same
490 sign in almost all of the oceanic regions in line with the assumption of nitrification begin
491 the dominant contribution to N_2O production. Changes in N_2O production in the
492 subsurface are translated into corresponding changes in N_2O flux. There is only one
493 oceanic region (Sub-Polar Pacific) where this correlation does not occur. N_2O inventory
494 increases in all of the oceanic regions. The increase in inventory is particularly
495 pronounced at low latitudes along the eastern boundary currents in the Equatorial and
496 Tropical Pacific, Indian Ocean and also in smaller quantities in the Atlantic Ocean.
497 Figure 7 shows how the decrease in N_2O production and increase in N_2O storage occurs
498 in all oceanic basins.
499 The synergy among the driving mechanisms can be explored with a box model pursuing

two objectives. First, to separate the effect of physical (i.e., increased stratification) and the biogeochemical (i.e., reduction of N_2O production in the high-O_2 regions) mechanisms on N_2O emissions. In this way we can reproduce future projections assuming that the only mechanisms ruling the N_2O dynamics in the future were those that we have proposed in our hypothesis, i.e., increased stratification and reduction of N_2O production in high-O_2 regions. Secondly, to explore a wider range of values for both mixing (i.e., degree of stratification) and efficiency of N_2O production in high-O_2 conditions. In the particular NEMO-PISCES model projection we have studied, changes in mixing and export are unique and can not be explored individually.

To this end, a box model was designed to explore the response of oceanic N_2O emissions to changes in export of organic matter (hence N_2O production only in high-O_2 conditions) and changes in the mixing ratio between deep (> 100m) and surface (< 100m) layers. We divided the water column into two compartments: a surface layer in the upper 100m where 80% of surface N_2O concentration is outgassed to the atmosphere (Eq. (3)), and a deeper layer beyond 100m, where N_2O is produced from remineralization as a fraction of the organic matter exported in the ocean interior (Eq. (4)). The N_2O reservoirs in the surface and in the deep layer are allowed to exchange. The exchange is regulated by a mixing coefficient v:

$$\text{surface } N_2O\ ; \quad \frac{dN_2O^s}{dt} = -v \cdot (N_2O^s - N_2O^d) - \kappa \cdot N_2O^s \tag{3}$$

$$\text{deep } N_2O\ ; \quad \frac{dN_2O^d}{dt} = v \cdot (N_2O^s - N_2O^d) + \varepsilon \cdot \Phi^{POC} \tag{4}$$

where N_2O^s is N_2O in the surface, N_2O^d is N_2O in the deep reservoir, Φ^{POC} is the flux of POC into the lower compartment, v is the mixing coefficient between both compartments, k is the fraction of N_2O^s outgassed to the atmosphere and e the fraction of POC leading to N_2O^d formation (Fig. S3 and Table S1, Supplementary Material). Equations (3) and (4) are solved for a combination of POC fluxes and mixing coefficients, reflecting the increasing stratification and the decrease in export production projected by year 2100 (Sarmiento et al., 2004; Bopp et al., 2013).

A decrease in the N_2O flux is observed for a wide range of boundary conditions simulating reduced mixing and export of POC (Fig. 8a). The most extreme scenario explored with the box model suggests a -20% decrease in N_2O flux, although these

associated values of mixing and export are clearly unrealistic, from a nearly total stagnation of ocean circulation between the deep and surface layers to an attenuation of export of -20% in the global ocean.

The projected increase in N_2O storage in the deep reservoir is reproduced by the box model (Fig. 8b) at a wide range of changes particularly in mixing. Changes in mixing dominate over changes in export as drivers of the increase in the N_2O reservoir at depth. A 25% decrease in mixing leads to an increase in storage similar to the one projected with NEMO-PISCES (+10%), independently of changes in export of organic matter.

In general, the interplay between mixing and export of organic matter operates differently when N_2O flux or N_2O inventory are considered. The box model experiment suggests that the evolution of the N_2O reservoir is driven almost entirely by changes in mixing, while changes of mixing and export of organic matter have similar relevance when modulating N_2O emissions.

5. Caveats in estimating N_2O using ocean biogeochemical models

The state variables upon which representation of N_2O in models rely, i.e., oxygen and export of carbon, are compared to the CMIP5 model ensemble to put our analysis in context of the current state-of-the-art model capabilities. We focus here our analysis on suboxic waters ($O_2 < 5$ µmol L^{-1}) and on export production. Whereas CMIP5 models tend to have large volumes of O_2 concentrations in the suboxic regime, it is not the case for our NEMO-PISCES simulation, which clearly underestimates the volume of low-oxygen waters as compared to the oxygen corrected World Ocean Atlas 2005 (WOA2005*) (Bianchi et al., 2012). The fact that NEMO-PISCES forced by IPSL-CM5A-LR is highly oxygenated is confirmed by Figure 9, where the histogram of the full O_2 spectrum of WOA2005* and NEMO-PISCES is shown. The O_2 distribution in the model shows a deficient representation of the OMZs, with higher concentrations than those from observations. The rest of the O_2 spectrum is well represented in our model.

The O_2 distribution in the model (Fig. 10) shows a deficient representation of the OMZs, with higher concentrations than those from observations in WOA2005* and the other CMIP5 models. NEMO-PISCES is therefore biased towards the high O_2 production pathway of N_2O due to the modeled O_2 fields.

When turning to the export of organic matter, NEMO-PISCES is close to the CMIP5 average value of 6.9 PgC yr^{-1}. The overall distribution of export is also very similar to the CMIP5 model mean and both show smaller values than those from the data-based estimate of 9.84 PgC yr^{-1} from Dunne et al., 2007 (Fig. 10).

The uncertainties derived from present and future model projections can be estimated using the spread in the CMIP5 model projection of export of organic matter and assuming a linear response between nitrification (or export) and N_2O production in the subsurface, which is assumed to be quickly outgassed to the atmosphere. In NEMO-PISCES, a decrease in 13% in export leads to a maximum decrease in N_2O emissions of 12% in the P.OMZ scenario. Based on results by Bopp et al. (2013), changes in export of carbon span -7% to -18% in the CMIP5 model ensemble at the end of the 21st century and for RCP8.5. The spread would propagate to a similar range in projected N_2O emissions across the CMIP5 model ensemble. Applying these values to present N_2O emissions of 3.6 TgN yr^{-1}, uncertainties are then bracketed between -0.25 and -0.65 TgN yr^{-1}.

Regarding the low-O_2 pathway, a similar approach is not that straight forward. Zamora et al., (2012) found that a linear relationship between AOU and N_2O production might occur even at the OMZ of the ETP. Zamora et al. (2012) acknowledged the fact that the MEMENTO database includes N_2O advected from other regions and that mixing could play a relevant role, smoothing the fit between N_2O and AOU from exponential to linear. However, Zamora et al. (2012) quoting Frame and Casciotti (2010), suggested that regions were an exponential relationship in N_2O production is present might be rare, that other non-exponential N_2O production processes might occur and therefore the plot they presented could describe the actual linear relationship between N_2O production and oxygen consumption. Based on this hypothesis, we could refer again to the linear relationship suggested in the high-O_2 and export scenario. However, in this case the CMIP5 model projections of changes in the hypoxic and suboxic volumes differ substantially. Most models project an expansion of the OMZs in the +2% to +16% range in the suboxic volume (O_2 < 5 µmol L^{-1}). There are, however, models that project a slight reduction of 2%. Spatial variability of projections add to the spread between CMIP5 models. These discrepancies suggest that uncertainties from this spread must be interpreted with caution when estimating potential future N_2O emissions.

592 The use of O_2 consumption as a proxy for the actual N_2O production plays therefore a
593 pivotal role in the uncertainties in N_2O model estimations. Future model development
594 should aim at the implementation of mechanistic parameterizations of N_2O production
595 based on nitrification and denitrification rates. Further, in order to determine accurate
596 O_2 boundaries for both N_2O production and N_2O consumption at the core of OMZs
597 additional measurements and microbial experiments are needed. The contribution of the
598 high-O_2 pathway that was considered in this model analysis might be a conservative
599 estimate. Freing et al. (2012) suggested that the high-O_2 pathway could be responsible of
600 93% of the total N_2O production. Assuming that changes in the N_2O flux are mostly
601 driven by N_2O production via nitrification, that would suggest a larger reduction in the
602 marine N_2O emissions in the future. However, the mismatch between NEMO-PISCES
603 and the Nevison et al. (2004) spatial distribution of N_2O emissions in the western part of
604 the basins suggests that changes in the future might not be as big as those projected in the
605 model in such regions. Changes would be then distributed more homogeneously.
606 The model assumption neglecting N_2O production in the upper 100m avoids one
607 important source of uncertainty in estimating global oceanic N_2O fluxes. In case
608 nitrification occurs in the euphotic layer, our results would be facing a significant
609 uncertainty of at least ±25% in N_2O emissions according to Zamora and Oschlies (2014)
610 analysis using the UVic Earth System Climate Model. Finally, Zamora et al. (2012)
611 observed a higher than expected N_2O consumption at the core of the OMZ in the
612 Eastern Tropical Pacific, occurring at an upper threshold of 10 μmol L^{-1}. The
613 contribution of OMZs to total N_2O production remains an open question. N_2O
614 formation associated with OMZs might be counterbalanced by its own local
615 consumption, leading to the attenuation of the only increasing source of N_2O
616 attributable to the projected future expansion of OMZs (Steinacher et al., 2010; Bopp et
617 al., 2013).
618 The combined effect of climate change and ocean acidification has not been analyzed in
619 this study. N_2O production processes might be altered by the response of nitrification to
620 increasing levels of seawater pCO_2 (Huesemann et al., 2002; Beman et al. 2011). Beman
621 et al. (2011) reported a reduction in nitrification in response to decreasing pH. This
622 result suggests that N_2O production might decrease beyond what we have estimated only
623 due to climate change. Conversely, negative changes in the ballast effect could potentially

624 reinforce nitrification at shallow depth in response to less efficient POC export to depth
625 and shallow remineralization (Gehlen et al., 2011). Regarding N_2O formation via
626 denitrification, changes in seawater pH as a consequence of higher levels of CO_2 might
627 not be substantial enough to change the N_2O production efficiency, assuming a similar
628 response of marine denitrifiers as reported for denitrifying bacteria have in terrestrial
629 systems (Liu et al., 2010). Finally, the C:N ratio in export production (Riebesell et al.,
630 2007) might increase in response to ocean acidification, potentially leading to a greater
631 expansion of OMZs than simulated here (Oschlies et al., 2008; Tagliabue et al., 2011),
632 and therefore to enhanced N_2O production associated with the low-O_2 pathway.
633 Changes in atmospheric nitrogen deposition have not been considered in this study. It
634 has been suggested that due to anthropogenic activities the additional amount of reactive
635 nitrogen in the ocean could fuel primary productivity and N_2O production. Estimates are
636 however low, around 3-4% of the total oceanic emissions (Suntharalingam et al., 2012).
637 Longer simulation periods could reveal additional effects on N_2O transport beyond
638 changes in upwelling or meridional transport of N_2O in the subsurface (Suntharalingam
639 and Sarmiento, 2000) that have been observed in this transient simulation. Long-term
640 responses might include eventual ventilation of the N_2O reservoir in the Southern Ocean,
641 highlighting the role of upwelling regions as an important source of N_2O when longer
642 time periods are considered in model projections. Additional studies using other ocean
643 biogeochemical models might also yield alternative values using the same
644 parameterizations. N_2O production is particularly sensitive to the distribution and
645 magnitude of export of organic matter and O_2 fields defined in models.
646
647 6. Contribution of future N_2O to climate feedbacks
648
649 Changes in the oceanic emissions of N_2O to the atmosphere will have an impact on
650 atmospheric radiative forcing, with potential feedbacks on the climate system. Based on
651 the estimated 4 to 12% decrease in N_2O sea-to-air flux over the 21st century under
652 RCP8.5, we estimated the feedback factor for these changes as defined by Xu-Ri et al.
653 (2012). Considering the reference value of the pre-industrial atmospheric N_2O
654 concentration of 280 ppb in equilibrium, and its associated global N_2O emissions of 11.8
655 TgN yr^{-1}, we quantify the resulting changes in N_2O concentration per degree for the two

projected emissions in 2100 using P.TEMP and P.OMZ. The model projects changes in N_2O emissions of -0.16 and -0.48 TgN yr^{-1} respectively, whereas surface temperature is assumed to increase globally by 3°C on average according to the physical forcing used in our simulations. These results yield -0.05 and -0.16 TgN yr^{-1} K^{-1}, or alternatively -1.25 and -3.80 ppb K^{-1} for P.TEMP and P.OMZ respectively. Using Joos et al. (2001) we calculate the feedback factor in equilibrium for projected changes in emissions to be -0.005 and -0.014 W $m^{-2}K^{-1}$ in P.TEMP and P.OMZ.

Stocker et al. (2013) projected changes in terrestrial N_2O emissions in 2100 using transient model simulations leading to feedback strengths between +0.001 and +0.015 W $m^{-2}K^{-1}$. Feedback strengths associated with the projected decrease of oceanic N_2O emissions are of the same order of magnitude as those attributable to changes in the terrestrial sources of N_2O, yet opposite in sign, suggesting a compensation of changes in radiative forcing due to future increasing terrestrial N_2O emissions. At this stage, potential compensation between land and ocean emissions is to be taken with caution, as it relies of a single model run with constant atmospheric N_2O.

7. Conclusions

Our simulations suggest that anthropogenic climate change could lead to a global decrease in oceanic N_2O emissions during the 21st century. This maximum projected decrease of 12% in marine N_2O emissions for the business-as-usual high CO_2 emissions scenario would compensate for the estimated increase in N_2O fluxes from the terrestrial biosphere in response to anthropogenic climate change (Stocker et al. 2013), so that the climate-N_2O feedback may be more or less neutral over the coming decades.

The main mechanisms contributing to the reduction of marine N_2O emissions are a decrease in N_2O production in high oxygenated waters as well as an increase in ocean vertical stratification that acts to decrease the transport of N_2O from the sub-surface to the surface ocean. Despite the decrease in both N_2O production and N_2O emissions, simulations suggest that the global marine N_2O inventory may increase from 2005 to 2100. This increase is explained by the reduced transport of N_2O from the production zones to the air-sea interface.

Differences between the two parameterizations used here are more related to

688 biogeochemistry rather than changes in ocean circulation. Despite sharing the high-O_2
689 N_2O production pathway, leading to a decrease in N_2O emissions in both cases, the role
690 of warming in P.TEMP or higher N_2O yields at low-O_2 concentrations in P.OMZ
691 translate into notable differences in the evolution of the two production pathways.
692 However, the dominant effect of changes in stratification in both parameterizations
693 drives ultimately the homogeneous response of the parameterizations considered in
694 model projections in the next century.
695 The N_2O production pathways demand however a better understanding in order to
696 enable an improved representation of processes in models. At a first order, the efficiencies
697 of the production processes in response to higher temperatures or increased seawater
698 pCO_2 are required. Second order effects such as changes in the O_2 boundaries at which
699 nitrification and denitrification occur must be also taken into account. In the absence of
700 process-based parameterizations, N_2O production parameterizations will still rely on
701 export of organic carbon and oxygen levels. Both need to be improved in global
702 biogeochemical models.
703 The same combination of mechanisms (i.e., change in export production and ocean
704 stratification) have been identified as drivers of changes in oceanic N_2O emissions during
705 the Younger Dryas by Goldstein et al. (2003). The N_2O flux decreased, while the N_2O
706 reservoir was fueled by longer residence times of N_2O caused by increased stratification.
707 Other studies point towards changes in the N_2O production at the OMZs as the main
708 reason for variations in N_2O observed in the past (Suthhof et al., 2001). Whether these
709 mechanisms are plausible drivers of changes beyond year 2100 remains an open question
710 that needs to be addressed with longer simulations.
711

8. Acknowledgements

We thank Cynthia Nevison for providing us the N_2O sea-to-air flux dataset. We thank Annette Kock and Herman Bange for the availability of the MEMENTO database (https://memento.geomar.de). We thank Christian Ethé for help analyzing PISCES model drift. Comments by Parvadha Suntharalingam and three anonymous reviewers improved significantly this manuscript. Nicolas Gruber acknowledges the support of ETH Zürich. This work has been supported by the European Union via the Greencycles II FP7-PEOPLE-ITN-2008, number 238366.

721 7. References

722

723 Aumont, O., and Bopp, L.: Globalizing results from ocean in situ iron fertilization studies,
724 Global Biogeochemical Cycles, GB2017, 20, 10.1029/2005gb002591, 2006.
725 Bange, H. W., Rixen, T., Johansen, A. M., Siefert, R. L., Ramesh, R., Ittekkot, V., Hoffmann,
726 M. R., and Andreae, M. O.: A revised nitrogen budget for the Arabian Sea, Global
727 Biogeochemical Cycles, 14, 1283-1297, 10.1029/1999gb001228, 2000.
728 Bange, H. W., Bell, T. G., Cornejo, M., Freing, A., Uher, G., Upstill-Goddard, R. C., and
729 Zhang, G.: MEMENTO: a proposal to develop a database of marine nitrous oxide and methane
730 measurements, Environmental Chemistry, 6, 195-197, 10.1071/en09033, 2009.
731 Beman, J. M., Chow, C.-E., King, A. L., Feng, Y., Fuhrman, J. A., Andersson, A., Bates, N. R.,
732 Popp, B. N., and Hutchins, D. A.: Global declines in oceanic nitrification rates as a consequence
733 of ocean acidification, Proceedings of the National Academy of Sciences of the United States of
734 America, 108, 208-213, 10.1073/pnas.1011053108, 2011.
735 Bianchi, D., Dunne, J. P., Sarmiento, J. L., and Galbraith, E. D.: Data-based estimates of
736 suboxia, denitrification, and N2O production in the ocean and their sensitivities to dissolved O-
737 2, Global Biogeochemical Cycles, 26, GB2009, 10.1029/2011gb004209, 2012.
738 Bindoff, N., Willebrand, J., Artale, V., Cazenave, A., Gregory, J., Gulev, S., Hanawa, K.,
739 Le Quere, C., Levitus, S., Norjiri, Y., Shum, C., Talley, L., and Unnikrishnan, A.:
740 Observations: Oceanic Climate Change and Sea Level, In Climate Change 2007: The
741 Physical Science Basis.Contribution of Working Group I to the Fourth Assessment
742 Report of the Intergovernmental Panel on Climate Change, 2007.
743 Bopp, L., Resplandy, L., Orr, J. C., Doney, S. C., Dunne, J. P., Gehlen, M., Halloran, P.,
744 Heinze, C., Ilyina, T., Seferian, R., Tjiputra, J., and Vichi, M.: Multiple stressors of ocean
745 ecosystems in the 21st century: projections with CMIP5 models, Biogeosciences, 10, 6225-6245,
746 10.5194/bg-10-6225-2013, 2013.
747 Butler, J. H., Elkins, J. W., Thompson, T. M., and Egan, K. B.: Tropospheric and dissolved
748 N_2O of the west pacific and east-indian oceans during the el-nino southern oscillation event of
749 1987, Journal of Geophysical Research-Atmospheres, 94, 14865-14877,
750 10.1029/JD094iD12p14865, 1989.
751 Ciais, P., Sabine, C., Bala, G., Bopp, L., Brovkin, V., Canadell, J., Chhabra, A., DeFries,
752 R., Galloway, J., Heimann, M., Jones, C., Le Quéré, C., Myneni, RB., Piao, S. and

753 Thornton, P.: Carbon and Other Biogeochemical Cycles. In: Climate Change 2013: The
754 Physical Science Basis. Contribution of Working Group I to the Fifth Assessment Report
755 of the Intergovernmental Panel on Climate Change, 2013.
756 Cocco, V., Joos, F., Steinacher, M., Froelicher, T. L., Bopp, L., Dunne, J., Gehlen, M., Heinze,
757 C., Orr, J., Oschlies, A., Schneider, B., Segschneider, J., and Tjiputra, J.: Oxygen and indicators
758 of stress for marine life in multi-model global warming projections, Biogeosciences, 10, 1849-
759 1868, 10.5194/bg-10-1849-2013, 2013.
760 Cohen, Y., and Gordon, L. I.: Nitrous-oxide in oxygen minimum of eastern tropical north
761 pacific - evidence for its consumption during denitrification and possible mechanisms for its
762 production, Deep-Sea Research, 25, 509-524, 10.1016/0146-6291(78)90640-9, 1978.
763 Cohen, Y., and Gordon, L. I.: Nitrous-oxide production in the ocean, Journal of Geophysical
764 Research-Oceans and Atmospheres, 84, 347-353, 10.1029/JC084iC01p00347, 1979.
765 Crutzen, P. J.: Influence of nitrogen oxides on atmospheric ozone content, Quarterly Journal of
766 the Royal Meteorological Society, 96, 320-326, 10.1002/qj.49709640815, 1970.
767 de Wilde, H. P. J., and de Bie, M. J. M.: Nitrous oxide in the Schelde estuary: production by
768 nitrification and emission to the atmosphere, Marine Chemistry, 69, 203-216, 10.1016/s0304-
769 4203(99)00106-1, 2000.
770 Deutsch, C., Brix, H., Ito, T., Frenzel, H., and Thompson, L.: Climate-Forced Variability of
771 Ocean Hypoxia, Science, 333, 336-339, 10.1126/science.1202422, 2011.
772 Dufresne, J. L., Foujols, M. A., Denvil, S., Caubel, A., Marti, O., Aumont, O., Balkanski, Y.,
773 Bekki, S., Bellenger, H., Benshila, R., Bony, S., Bopp, L., Braconnot, P., Brockmann, P.,
774 Cadule, P., Cheruy, F., Codron, F., Cozic, A., Cugnet, D., de Noblet, N., Duvel, J. P., Ethe, C.,
775 Fairhead, L., Fichefet, T., Flavoni, S., Friedlingstein, P., Grandpeix, J. Y., Guez, L., Guilyardi,
776 E., Hauglustaine, D., Hourdin, F., Idelkadi, A., Ghattas, J., Joussaume, S., Kageyama, M.,
777 Krinner, G., Labetoulle, S., Lahellec, A., Lefebvre, M. P., Lefevre, F., Levy, C., Li, Z. X., Lloyd,
778 J., Lott, F., Madec, G., Mancip, M., Marchand, M., Masson, S., Meurdesoif, Y., Mignot, J.,
779 Musat, I., Parouty, S., Polcher, J., Rio, C., Schulz, M., Swingedouw, D., Szopa, S., Talandier,
780 C., Terray, P., Viovy, N., and Vuichard, N.: Climate change projections using the IPSL-CM5
781 Earth System Model: from CMIP3 to CMIP5, Climate Dynamics, 40, 2123-2165,
782 10.1007/s00382-012-1636-1, 2013.
783 Dunne, J. P., Sarmiento, J. L., and Gnanadesikan, A.: A synthesis of global particle export
784 from the surface ocean and cycling through the ocean interior and on the seafloor, Global

785 Biogeochemical Cycles, 21, GB4006,10.1029/2006gb002907, 2007.
786 Elkins, J. W., Wofsy, S. C., McElroy, M. B., Kolb, C. E., and Kaplan, W. A.: Aquatic sources
787 and sinks for nitrous-oxide, Nature, 275, 602-606, 10.1038/275602a0, 1978.
788 Farias, L., Paulmier, A., and Gallegos, M.: Nitrous oxide and N-nutrient cycling in the
789 oxygen minimum zone off northern Chile, Deep-Sea Research Part I-Oceanographic
790 Research Papers, 54, 164-180, 10.1016/j.dsr.2006.11.003, 2007.
791 Fletcher, S. E. M., Gruber, N., Jacobson, A. R., Gloor, M., Doney, S. C., Dutkiewicz, S.,
792 Gerber, M., Follows, M., Joos, F., Lindsay, K., Menemenlis, D., Mouchet, A., Muller, S. A.,
793 and Sarmiento, J. L.: Inverse estimates of the oceanic sources and sinks of natural CO_2 and
794 the implied oceanic carbon transport, Global Biogeochemical Cycles, 21, GB1010,
795 10.1029/2006gb002751, 2007.
796 Frame, C. H., and Casciotti, K. L.: Biogeochemical controls and isotopic signatures of nitrous
797 oxide production by a marine ammonia-oxidizing bacterium, Biogeosciences, 7, 2695-2709,
798 10.5194/bg-7-2695-2010, 2010.
799 Freing, A., Wallace, D. W. R., Tanhua, T., Walter, S., and Bange, H. W.: North Atlantic
800 production of nitrous oxide in the context of changing atmospheric levels, Global
801 Biogeochemical Cycles, 23, GB4015, 10.1029/2009gb003472, 2009.
802 Freing, A., Wallace, D. W. R., and Bange, H. W.: Global oceanic production of nitrous oxide,
803 Philosophical Transactions of the Royal Society B-Biological Sciences, 367, 1245-1255,
804 10.1098/rstb.2011.0360, 2012.
805 Gehlen, M., Gruber, N., Gangstø, R., Bopp, L., and Oschlies, A.: Biogeochemical consequences
806 of ocean acidification and feedbacks to the earth system. Ocean acidification: 230-248, 2011.
807 Goldstein, B., Joos, F., and Stocker, T. F.: A modeling study of oceanic nitrous oxide during the
808 Younger Dryas cold period, Geophysical Research Letters, 30, 1092, 10.1029/2002gl016418,
809 2003.
810 Goreau, T. J., Kaplan, W. A., Wofsy, S. C., McElroy, M. B., Valois, F. W., and Watson, S. W.:
811 Production of NO_2^- and N_2O by nitrifying bacteria at reduced concentrations of oxygen, Applied
812 and Environmental Microbiology, 40, 526-532, 1980.
813 Gruber, N., and Galloway, J. N.: An Earth-system perspective of the global nitrogen cycle,
814 Nature, 451, 293-296, 10.1038/nature06592, 2008.
815 Gruber, N.: Warming up, turning sour, losing breath: ocean biogeochemistry under global
816 change, Philosophical Transactions of the Royal Society a-Mathematical Physical and
817 Engineering Sciences, 369, 1980-1996, 10.1098/rsta.2011.0003, 2011.

818 Gruber, N.: The marine nitrogen cycle: Overview of distributions and processes. In:
819 Nitrogen in the marine environment, 2nd edition, 1-50, 2008.
820 Huesemann, M. H., Skillman, A. D., and Crecelius, E. A.: The inhibition of marine nitrification
821 by ocean disposal of carbon dioxide, Marine Pollution Bulletin, 44, 142-148, 10.1016/s0025-
822 326x(01)00194-1, 2002.
823 Jin, X., and Gruber, N.: Offsetting the radiative benefit of ocean iron fertilization by enhancing
824 N_2O emissions, Geophysical Research Letters, 30, 2249, 10.1029/2003gl018458, 2003.
825 Johnston, H.: Reduction of stratospheric ozone by nitrogen oxide catalysts from supersonic
826 transport exhaust, Science, 173, 517-522, 10.1126/science.173.3996.517, 1971.
827 Joos, F., Prentice, I. C., Sitch, S., Meyer, R., Hooss, G., Plattner, G. K., Gerber, S., and
828 Hasselmann, K.: Global warming feedbacks on terrestrial carbon uptake under the
829 Intergovernmental Panel on Climate Change (IPCC) emission scenarios, Global Biogeochemical
830 Cycles, 15, 891-907, 10.1029/2000gb001375, 2001.
831 Keeling, R. F., Koertzinger, A., and Gruber, N.: Ocean Deoxygenation in a Warming World,
832 Annual Review of Marine Science, 2, 199-229, 10.1146/annurev.marine.010908.163855, 2010.
833 Liu, B., Morkved, P. T., Frostegard, A., and Bakken, L. R.: Denitrification gene pools,
834 transcription and kinetics of NO, N_2O and N-2 production as affected by soil pH, Fems
835 Microbiology Ecology, 72, 407-417, 10.1111/j.1574-6941.2010.00856.x, 2010.
836 Mantoura, R. F. C., Law, C. S., Owens, N. J. P., Burkill, P. H., Woodward, E. M. S., Howland,
837 R. J. M., and Llewellyn, C. A.: Nitrogen biogeochemical cycling in the northwestern indian-
838 ocean, Deep-Sea Research Part II-Topical Studies in Oceanography, 40, 651-671, 1993.
839 Myhre, G., Shindell, D., Bréon, F.-M., Collins, W., Fuglestvedt, J., Huang, J., Koch, D.,
840 Lamarque, J.-F., Lee, D., Mendoza, B., Nakajima, T., Robock, A., Stephens, G.,
841 Takemura, T. and Zhang, H.: Anthropogenic and Natural Radiative Forcing. In:
842 Climate Change 2013: The Physical Science Basis. Contribution of Working Group I to
843 the Fifth Assessment Report of the Intergovernmental Panel on Climate Change, 2013.
844 Nevison, C. D., Lueker, T. J., and Weiss, R. F.: Quantifying the nitrous oxide source
845 from coastal upwelling, Global Biogeochemical Cycles, 18, GB1018,
846 10.1029/2003gb002110, 2004.
847 Nevison, C., Butler, J. H., and Elkins, J. W.: Global distribution of N_2O and the Delta N_2O-
848 AOU yield in the subsurface ocean, Global Biogeochemical Cycles, 17, 1119,
849 10.1029/2003gb002068, 2003.

Nevison, C. D., Weiss, R. F., and Erickson, D. J.: Global oceanic emissions of nitrous-oxide, Journal of Geophysical Research-Oceans, 100, 15809-15820, 10.1029/95jc00684, 1995.

Oschlies, A., Schulz, K. G., Riebesell, U., and Schmittner, A.: Simulated 21st century's increase in oceanic suboxia by CO2-enhanced biotic carbon export, Global Biogeochemical Cycles, 22, GB4008, 10.1029/2007gb003147, 2008.

Prather, M. J., Holmes, C. D., and Hsu, J.: Reactive greenhouse gas scenarios: Systematic exploration of uncertainties and the role of atmospheric chemistry, Geophysical Research Letters, 39, L09803, 10.1029/2012gl051440, 2012.

Punshon, S., and Moore, R. M.: Nitrous oxide production and consumption in a eutrophic coastal embayment, Marine Chemistry, 91, 37-51, 10.1016/j.marchem.2004.04.003, 2004.

Ravishankara, A. R., Daniel, J. S., and Portmann, R. W.: Nitrous Oxide (N2O): The Dominant Ozone-Depleting Substance Emitted in the 21st Century, Science, 326, 123-125, 10.1126/science.1176985, 2009.

Resplandy, L., Levy, M., Bopp, L., Echevin, V., Pous, S., Sarma, V. V. S. S., and Kumar, D.: Controlling factors of the oxygen balance in the Arabian Sea's OMZ, Biogeosciences, 9, 5095-5109, 10.5194/bg-9-5095-2012, 2012.

Riebesell, U., Schulz, K. G., Bellerby, R. G. J., Botros, M., Fritsche, P., Meyerhoefer, M., Neill, C., Nondal, G., Oschlies, A., Wohlers, J., and Zoellner, E.: Enhanced biological carbon consumption in a high CO2 ocean, Nature, 450, 545-548, 10.1038/nature06267, 2007.

Sarmiento, J. L., Slater, R., Barber, R., Bopp, L., Doney, S. C., Hirst, A. C., Kleypas, J., Matear, R., Mikolajewicz, U., Monfray, P., Soldatov, V., Spall, S. A., and Stouffer, R.: Response of ocean ecosystems to climate warming, Global Biogeochemical Cycles, 18, GB3003, 10.1029/2003gb002134, 2004.

Steinacher, M., Joos, F., Frolicher, T. L., Bopp, L., Cadule, P., Cocco, V., Doney, S. C., Gehlen, M., Lindsay, K., Moore, J. K., Schneider, B., and Segschneider, J.: Projected 21st century decrease in marine productivity: a multi-model analysis, Biogeosciences, 7, 979-1005, 2010.

Stocker, B. D., Roth, R., Joos, F., Spahni, R., Steinacher, M., Zaehle, S., Bouwman, L., Xu, R., and Prentice, I. C.: Multiple greenhouse-gas feedbacks from the land biosphere under future climate change scenarios, Nature Climate Change, 3, 666-672, 10.1038/nclimate1864, 2013.

Suntharalingam, P., and Sarmiento, J. L.: Factors governing the oceanic nitrous oxide distribution: Simulations with an ocean general circulation model, Global Biogeochemical Cycles, 14, 429-454, 10.1029/1999gb900032, 2000.

882 Suntharalingam, P., Sarmiento, J. L., and Toggweiler, J. R.: Global significance of nitrous-oxide
883 production and transport from oceanic low-oxygen zones: A modeling study, Global
884 Biogeochemical Cycles, 14, 1353-1370, 10.1029/1999gb900100, 2000.
885 Suntharalingam, P., Buitenhuis, E., Le Quere, C., Dentener, F., Nevison, C., Butler, J. H.,
886 Bange, H. W., and Forster, G.: Quantifying the impact of anthropogenic nitrogen deposition on
887 oceanic nitrous oxide, Geophysical Research Letters, 39, L07605, 10.1029/2011gl050778, 2012.
888 Suthhof, A., Ittekkot, V., and Gaye-Haake, B.: Millennial-scale oscillation of denitrification
889 intensity in the Arabian Sea during the late Quaternary and its potential influence on
890 atmospheric N_2O and global climate, Global Biogeochemical Cycles, 15, 637-649,
891 10.1029/2000gb001337, 2001.
892 Tagliabue, A., Bopp, L., and Gehlen, M.: The response of marine carbon and nutrient cycles to
893 ocean acidification: Large uncertainties related to phytoplankton physiological assumptions,
894 Global Biogeochemical Cycles, 25, GB3017, 10.1029/2010gb003929, 2011.
895 Takahashi, T., Broecker, W. S., and Langer, S.: Redfield ratio based on chemical-data from
896 isopycnal surfaces, Journal of Geophysical Research-Oceans, 90, 6907-6924,
897 10.1029/JC090iC04p06907, 1985.
898 Tiedje, J.M.: Ecology of denitrification and dissimilatory nitrate reduction to
899 ammonium. Biology of anaerobic microorganisms, 179–244, 1988.
900 Wanninkhof, R.: Relationship between wind-speed and gas-exchange over the ocean, Journal of
901 Geophysical Research-Oceans, 97, 7373-7382, 10.1029/92jc00188, 1992.
902 Weiss, R. F., and Price, B. A.: Nitrous-oxide solubility in water and seawater, Marine Chemistry,
903 8, 347-359, 10.1016/0304-4203(80)90024-9, 1980.
904 Westley, M. B., Yamagishi, H., Popp, B. N., and Yoshida, N.: Nitrous oxide cycling in the
905 Black Sea inferred from stable isotope and isotopomer distributions, Deep-Sea Research Part
906 Ii-Topical Studies in Oceanography, 53, 1802-1816, 10.1016/j.dsr2.2006.03.012, 2006.
907 Yoshida, N., Morimoto, H., Hirano, M., Koike, I., Matsuo, S., Wada, E., Saino, T., and
908 Hattori, A.: Nitrification rates and N-15 abundances of N_2O and NO_3^- in the western north
909 pacific, Nature, 342, 895-897, 10.1038/342895a0, 1989.
910 Zamora, L. M., and Oschlies, A.: Surface nitrification: A major uncertainty in marine N_2O
911 emissions, Geophysical Research Letters, 41, 4247-4253, 10.1002/2014gl060556, 2014.
912 Zamora, L. M., Oschlies, A., Bange, H. W., Huebert, K. B., Craig, J. D., Kock, A., and
913 Loescher, C. R.: Nitrous oxide dynamics in low oxygen regions of the Pacific: insights from the
914 MEMENTO database, Biogeosciences, 9, 5007-5022, 10.5194/bg-9-5007-2012, 2012.

915 Zehr, J. P., and Ward, B. B.: Nitrogen cycling in the ocean: New perspectives on processes and
916 paradigms, Applied and Environmental Microbiology, 68, 1015-1024, 10.1128/aem.68.3.1015-
917 1024.2002, 2002.
918

919 Table 1: Standard deviation and correlation coefficients between P.TEMP and P.OMZ
920 parameterizations with respect to MEMENTO database observations (Bange et al., 2009).
921

	P.TEMP	P.OMZ	OBS
Standard deviation (in nmol N_2O L^{-1})	12	18	16
Correlation coefficient with obs.	0.49	0.42	-

922

923

Table S1: Box model boundary conditions and parameters. NEMO-PISCES model output values are taken from the historical averaged 1985 to 2005 time period and the future averaged 2080 to 2100 time period.

parameter	quantity	units	source
surface N_2O	10	TgN	PISCES model output
deep N_2O	1000	TgN	PISCES model output
yield N_2O produced from POC (e)	0.0025	mol N_2O /mol C	Nevison et al. (2003)
ratio of surface N_2O outgassed (π)	0.8	mol N_2O air/mol N_2O surface	assumption that most of the surface N_2O is outgassed.
ratio of surface N_2O exchanged with the deep N_2O compartment (v)	0.4	mol N_2O surface/ mol N_2O deep	box model assumption
export POC @100m in 2005	6.22	PgC yr^{-1}	PISCES model output
export POC @100m in 2100	5.30	PgC yr^{-1}	PISCES model output

924

925

926 Fig.1: N_2O sea-to-air flux (in mgN m^{-2} yr^{-1}) from (a) P.TEMP parameterzation averaged for the
927 1985 to 2005 time period in the historical simulation, (b) P.OMZ parameterization over the
928 same time period, (c) data product of Nevison et al. (2004) and (d) latitudinal N_2O sea-to-air
929 flux (in TgN $deg^{-1}yr^{-1}$) from Nevison et al. (2004) (black), P.TEMP (blue) and P.OMZ (red).

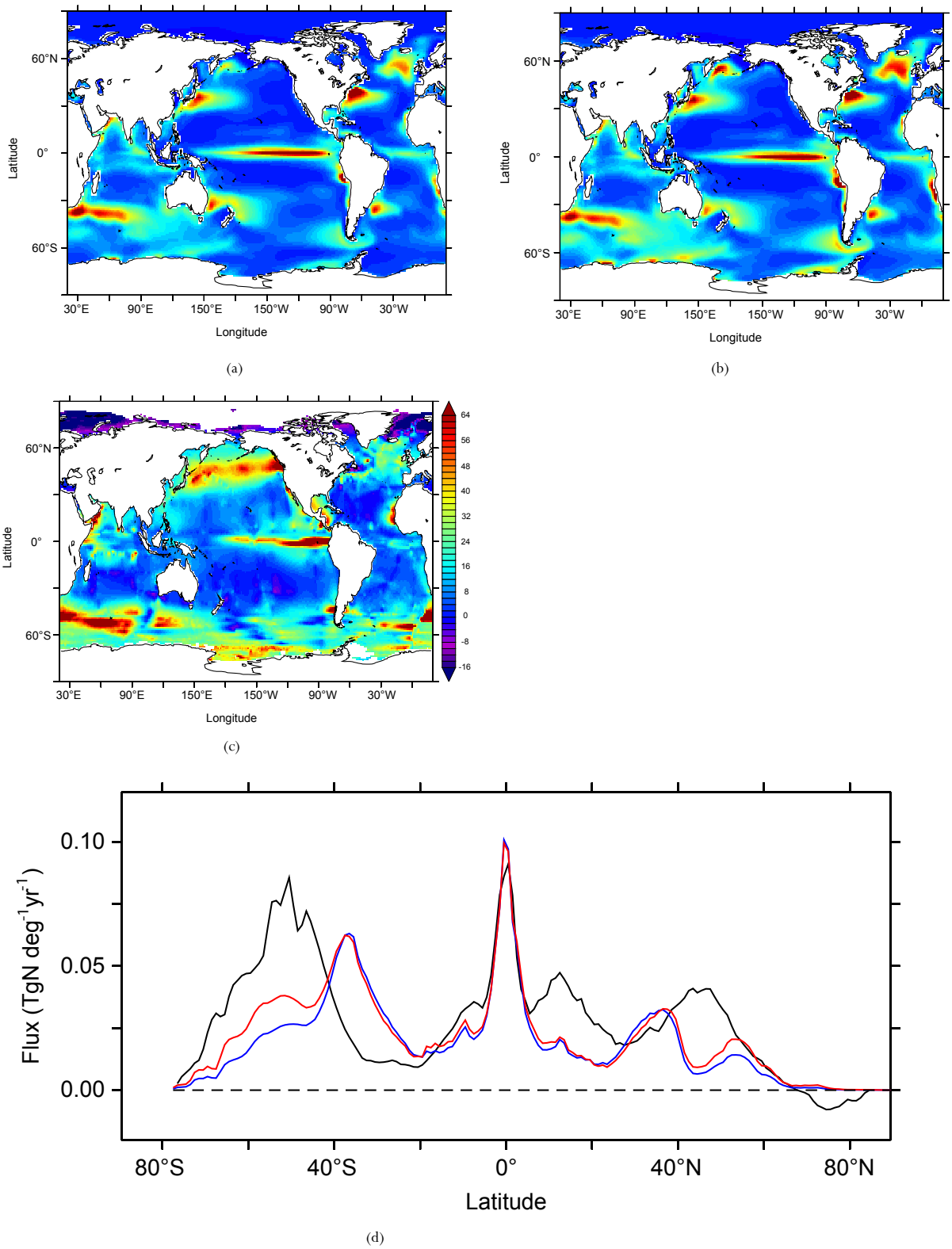

930
931
932
933
934

935 Fig.2: Global average depth profile of N_2O concentration (in nmol L^{-1}) from the MEMENTO
936 database (dots) (Bange et al., 2009), P.TEMP (blue) and P.OMZ (red). Model
937 parameterizations are averaged over the 1985 to 2005 time period from the historical
938 simulation.

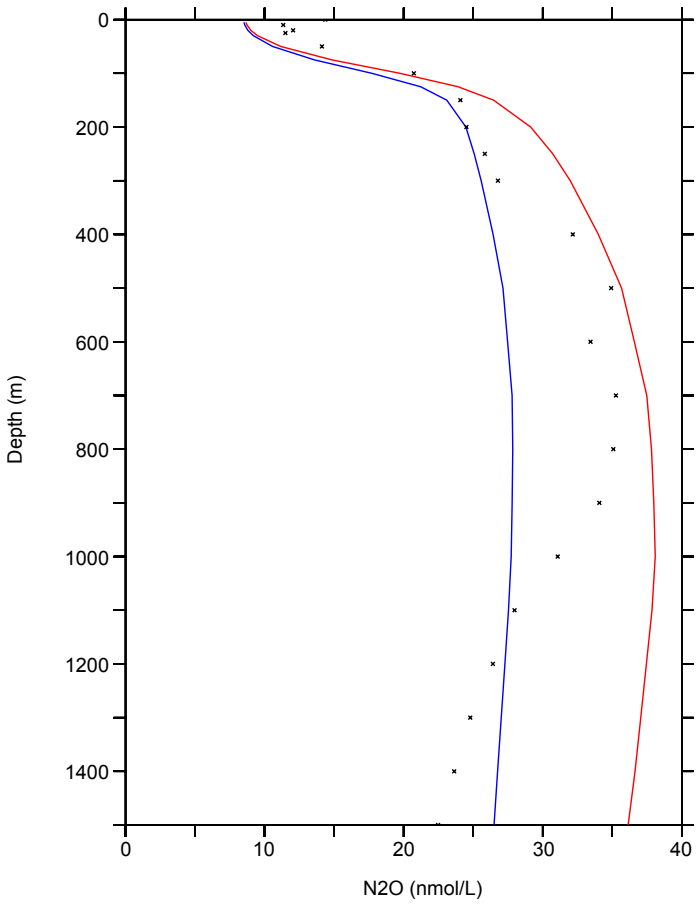

939
940

941 Fig.3: Relationship between O_2 concentration (in µmol L^{-1}) and N_2O concentration (in nmol L^{-1})
942 in the MEMENTO database (black) (Bange et al., 2009), compared to model (a) P.TEMP (blue)
943 and (b) P.OMZ (red) parameterizations averaged over the 1985 to 2005 time period from the
944 historical simulation.

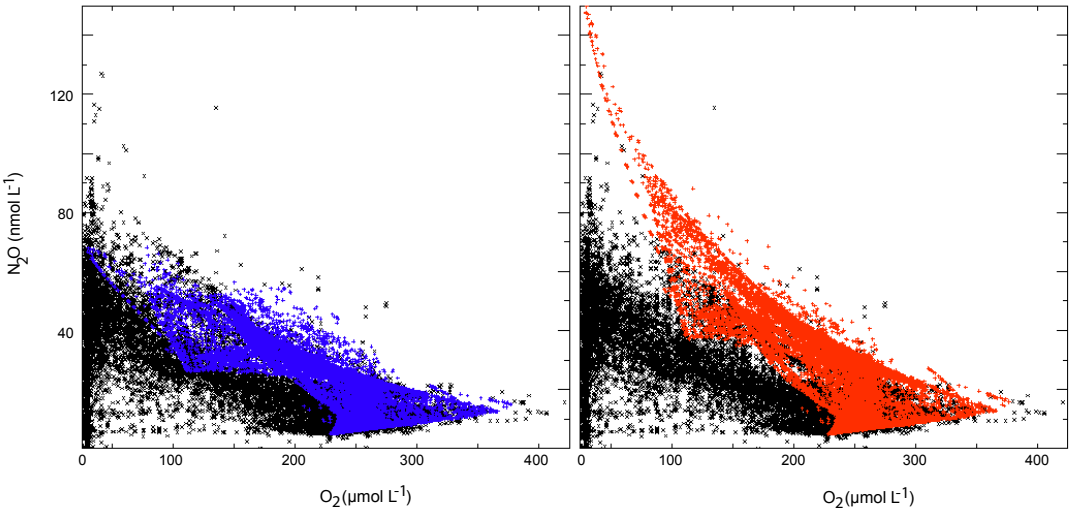

945
946
947 (a) (b)
948
949
950

Fig 4: (a) N_2O sea-to-air flux (in TgN yr^{-1}) from 1851 to 2100 in P.TEMP (blue) and P.OMZ (red) using the historical and future RCP8.5 simulations. Dashed lines indicate the mean value over the 1985 to 2005 time period. Change in N_2O sea-to-air flux (mgN $m^{-2}yr^{-1}$) from the averaged 2080-2100 to 1985-2005 time periods in future RCP8.5 and historical simulations in (b) P.TEMP and (c) P.OMZ parameterizations.

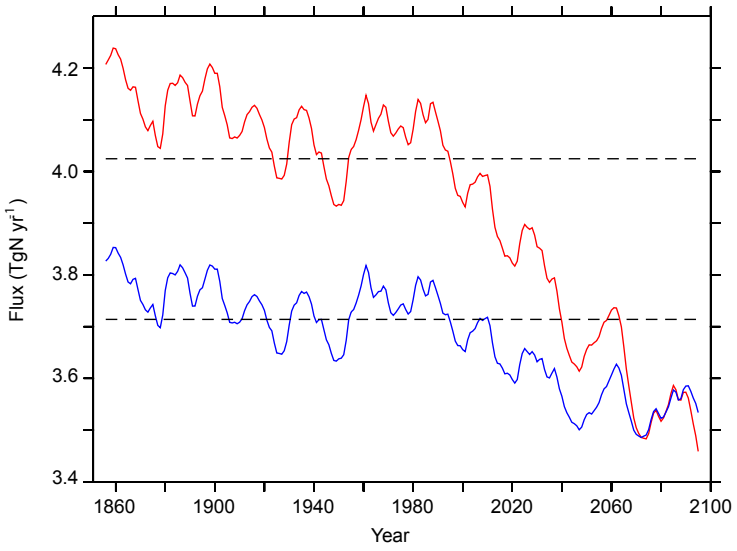

(a)

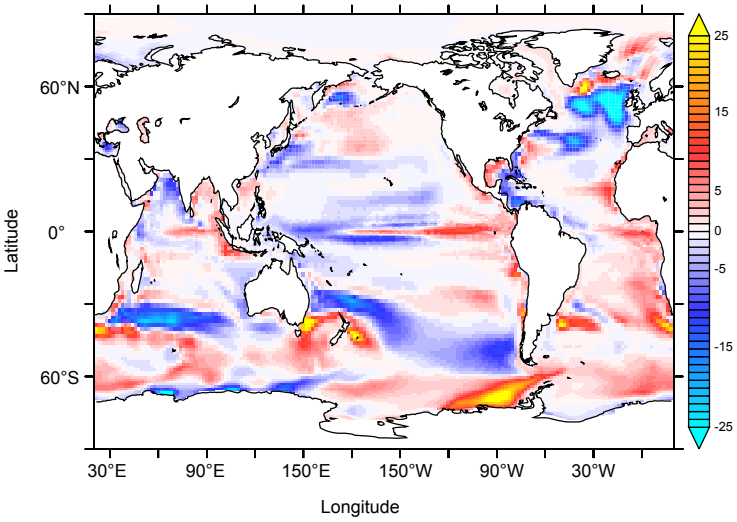

(b)

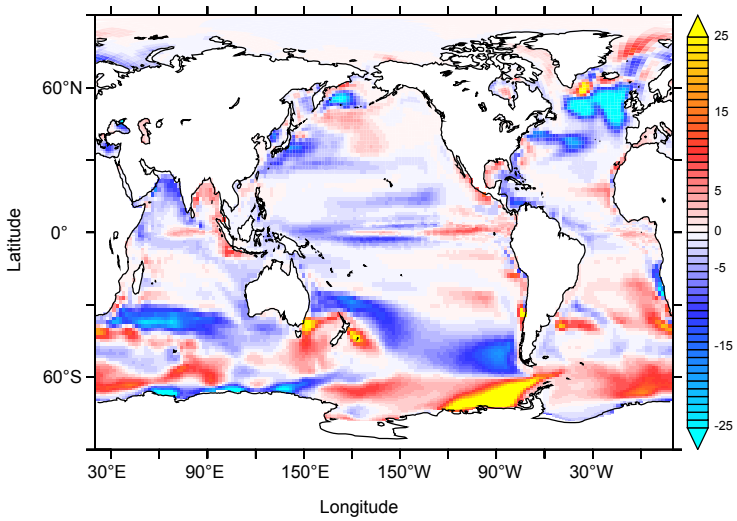
60°N
0°
60°S
Latitude
30°E
90°E
150°E
150°W
90°W
30°W
Longitude
25
15
5
0
-5
-15
-25

(c)

Fig 5: (a) Anomalies in export of organic matter at 100m (green), low-O_2 production pathway (short dashed red), high-O_2 production pathway (long dashed red) and total P.OMZ production (red) from 1851 to 2100 using the historical and future RCP8.5 simulations. (b) Anomalies in export of organic matter at 100m (green) and P.TEMP production (blue) over the same time period. (c) Change in high-O_2 production pathway of N_2O (in mgN m^{-2} yr^{-1}) in the upper 1500m between 2080-2100 to 1985-2005 averaged time periods. Hatched areas indicate regions where change in export of organic matter at 100m deep have the same sign as in changes in high-O_2 production pathway. (d) Change in low-O_2 production pathway of N_2O (in mgN m^{-2} yr^{-1}) in the upper 1500m between 2080-2100 to 1985-2005 averaged time periods. Hatched areas indicate regions where oxygen minimum zones (O_2 < 5 µmol L^{-1}) expand. (e) Volume (in 10^6 km^3) of hypoxic (black, O_2 < 60 µmol L^{-1}) and suboxic (red, O_2 < 5 µmol L^{-1}) areas in the 1851 to 2100 period in NEMO-PISCES historical and future RCP8.5 simulations.

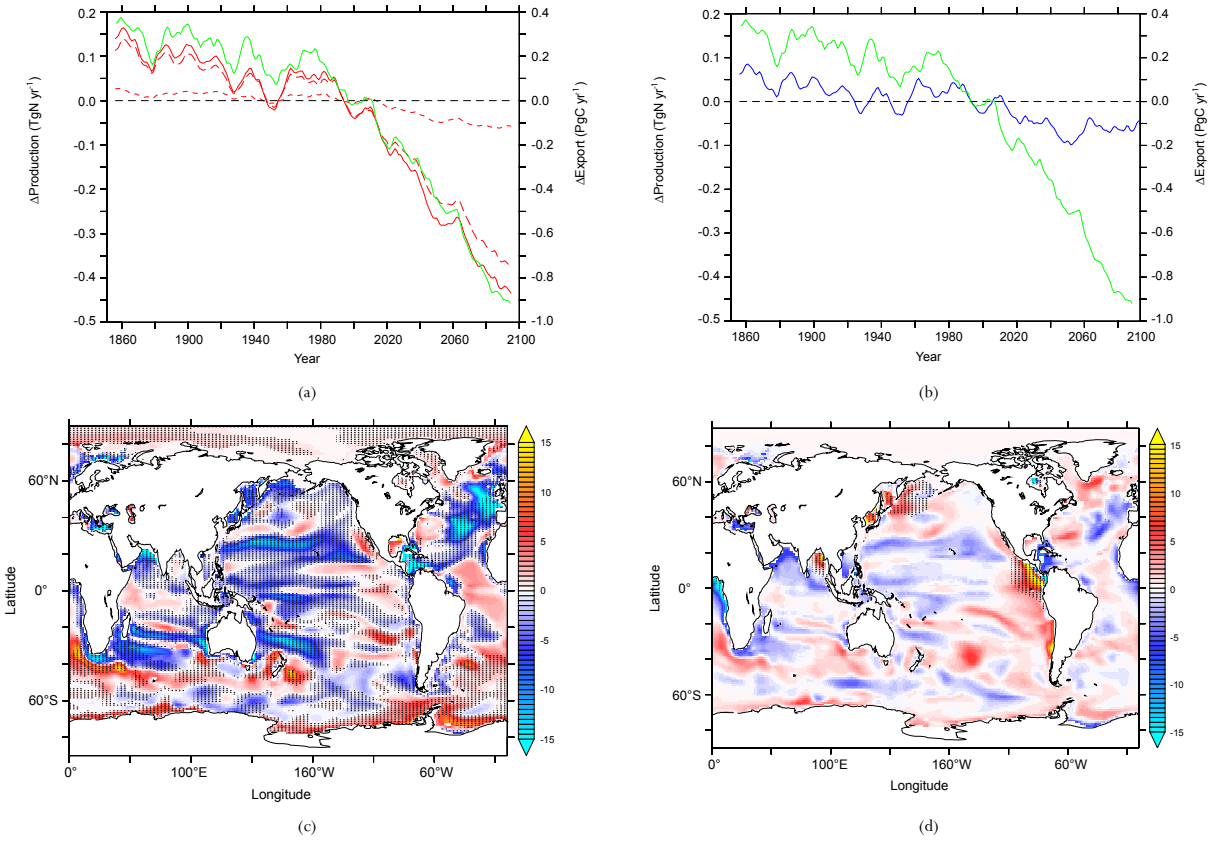

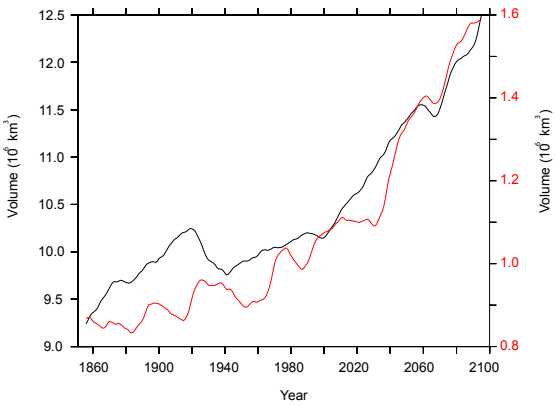
12.5
12.0
11.5
11.0
10.5
10.0
9.5
9.0
Volume (10^6 km^3)
1.6
1.4
1.2
1.0
0.8
Volume (10^6 km^3)
1860
1900
1940
1980
2020
2060
2100
Year

(e)

976
977

Fig 6: (a) Anomalies in N_2O inventory (in TgN) from 1851 to 2100 in P.TEMP (blue) and P.OMZ (red) using the historical and future RCP8.5 simulations in the upper 1500m. Change in vertically integrated N_2O concentration (in mgN m^{-2}) in the upper 1500m using NEMO-PISCES model mean from the averaged 2080-2100 to 1985-2005 time periods in future RCP8.5 and historical scenarios respectively in (b) P.TEMP and (c) P.OMZ. Hatched areas indicate regions where the annual mean mixed layer depth is reduced by more than 5m in 2080-2100 compared to 1985-2005.

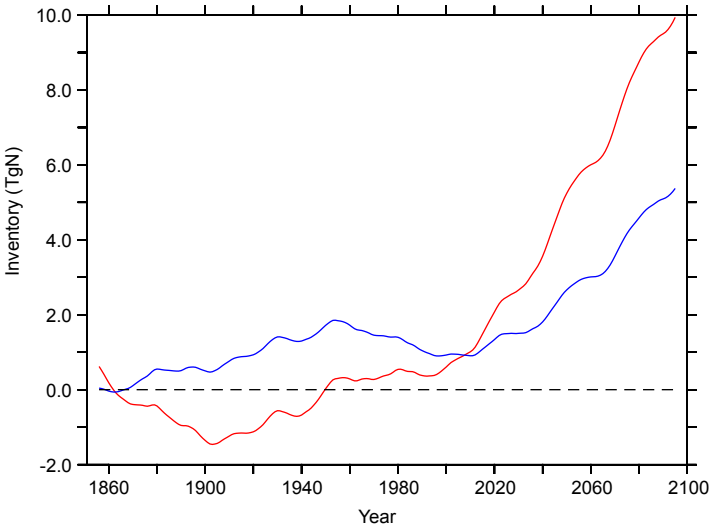

(a)

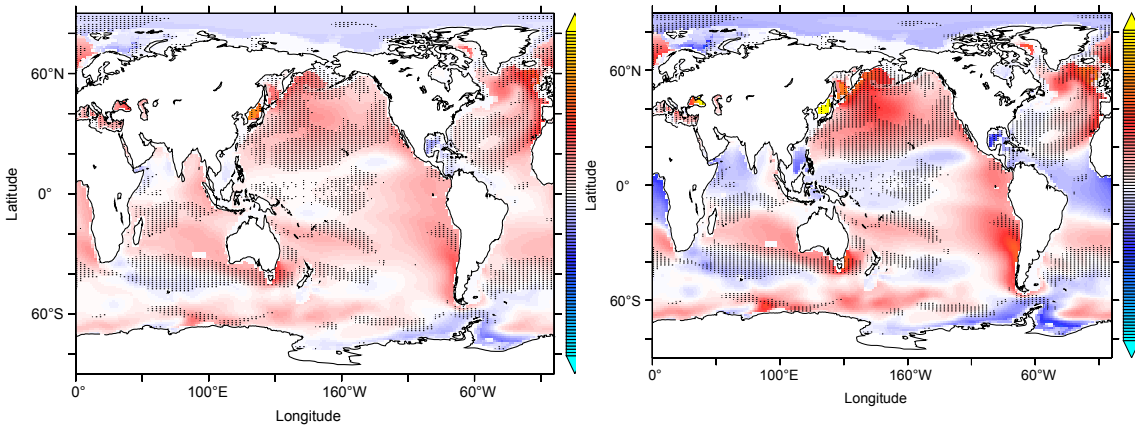

(b) (c)

990 Fig. 7: Change in the whole water column in N_2O sea-to-air flux (blue), high-O_2 production
991 pathway (red), low-O_2 production pathway (orange), total N_2O production (yellow) and N_2O
992 inventory (green) for P.OMZ from the averaged 2080-2100 to present 1985-2005 averaged
993 time period in the NEMO-PISCES historical and future RCP8.5 simulations (based on Mikaloff-
994 Fletcher et al. (2006) oceanic regions).

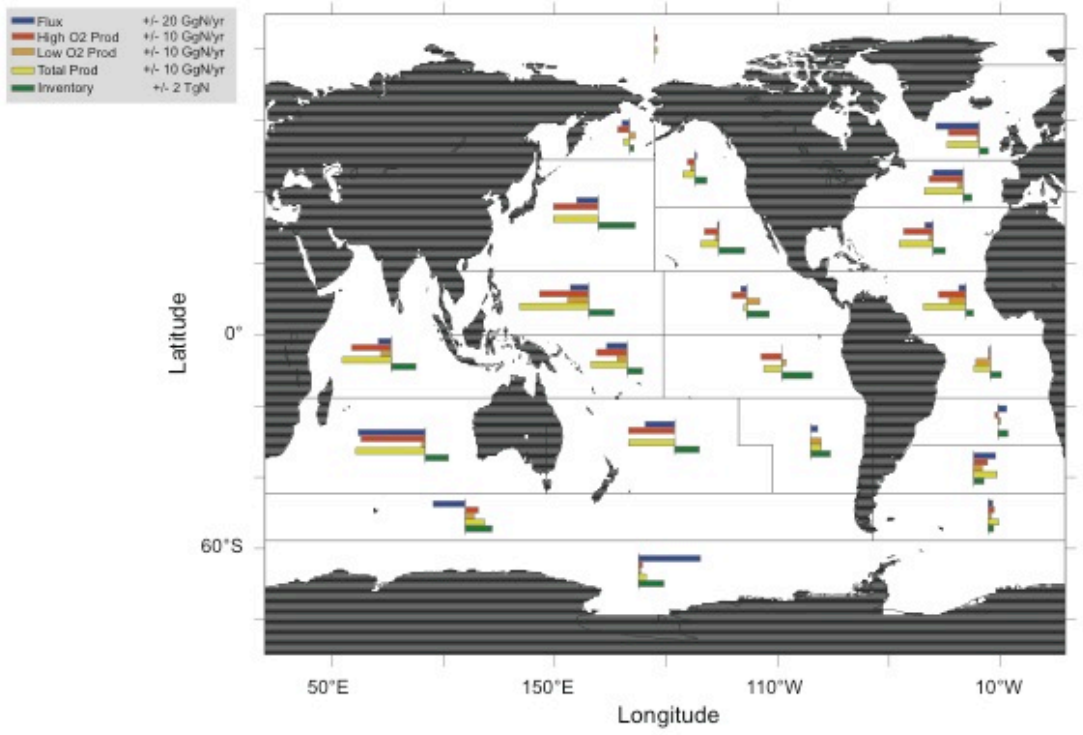

995
996

997 Fig. 8: Box model results, analyzing the effect of changes in ocean circulation by reducing the
998 mixing coefficient (μ in %) and changes in biogeochemistry by reducing export of organic
999 matter (in %) separately in N_2O sea-to-air emissions and N_2O inventory in 2100. (**a**) Constant
1000 regimes in percentage of the historical N_2O sea-to-air flux: 95% pink, 90% blue, 85% cyan and
1001 80% green, and (**b**) Constant regimes in percentage of the historical N_2O concentration in the
1002 deep: 90% pink, 110% blue, 125% cyan and 150% green.
1003

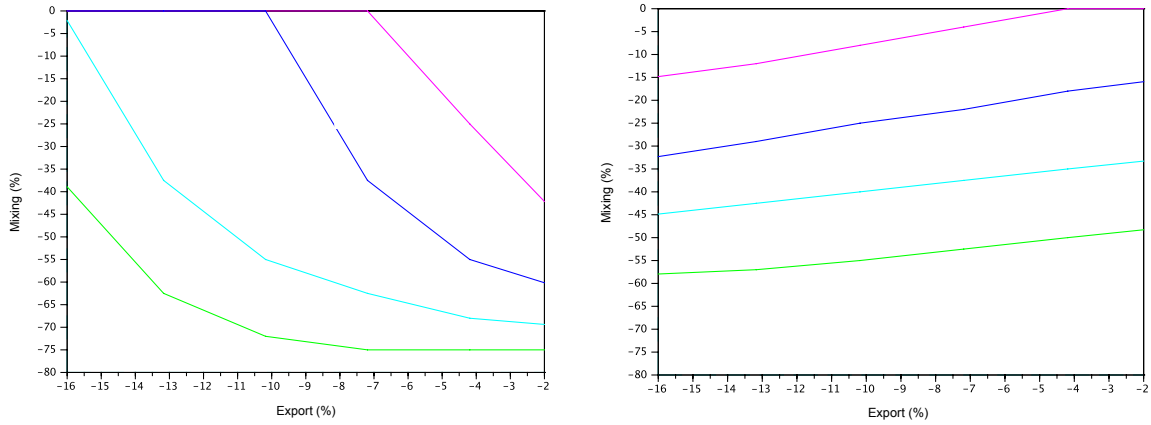

1004

1005 Figure 9: Distribution of O_2 concentration in NEMO-PISCES 1985 to 2005 averaged time
1006 period (black) compared to the oxygen-corrected World Ocean Atlas (red) from Bianchi et al.
1007 (2012). Interval widths are O_2 concentrations at steps of 5 µmol L^{-1}.

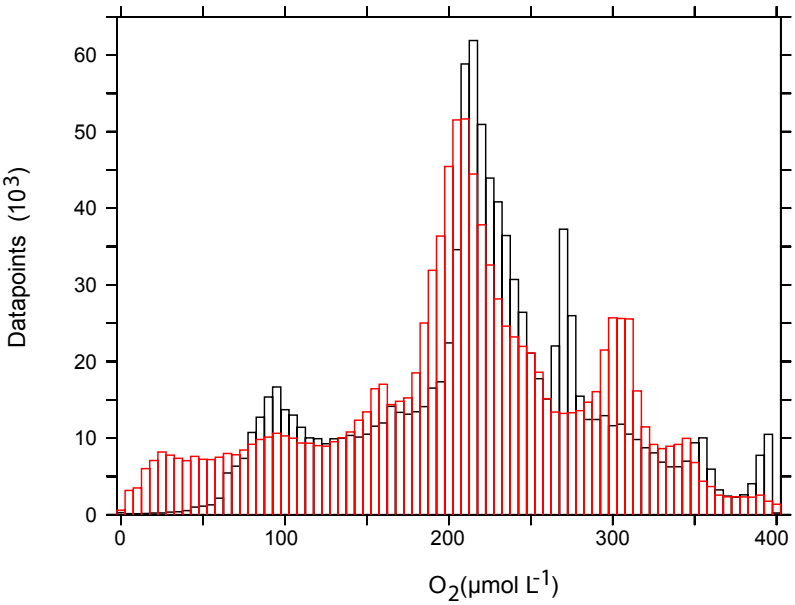

1008

1009

Figure 10: Averaged O_2 concentration between 200-600m depth (in µmol L^{-1}) (left) and export of carbon (in mmolC m^{-2} d^{-1}) (right) in (**a**) WOA2005* and Dunne et al. (2007), (**b**) CMIP5 model mean historical simulations over the 1985-2005 time period and (**c**) NEMO-PISCES for the present 1985-2005 time period.

a. WOA2005* and Dunne et al., 2007

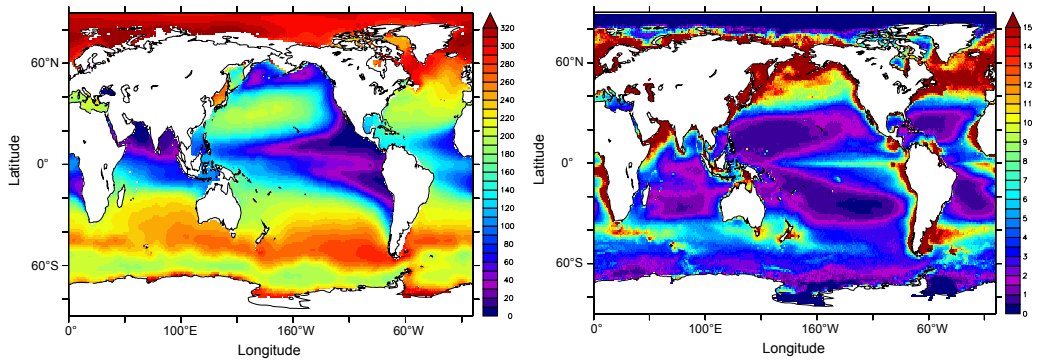

b. CMIP5 model mean

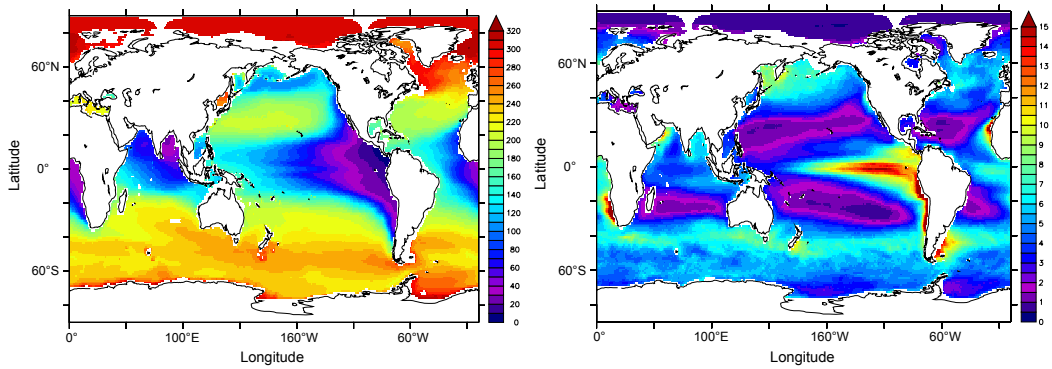

c. NEMO-PISCES

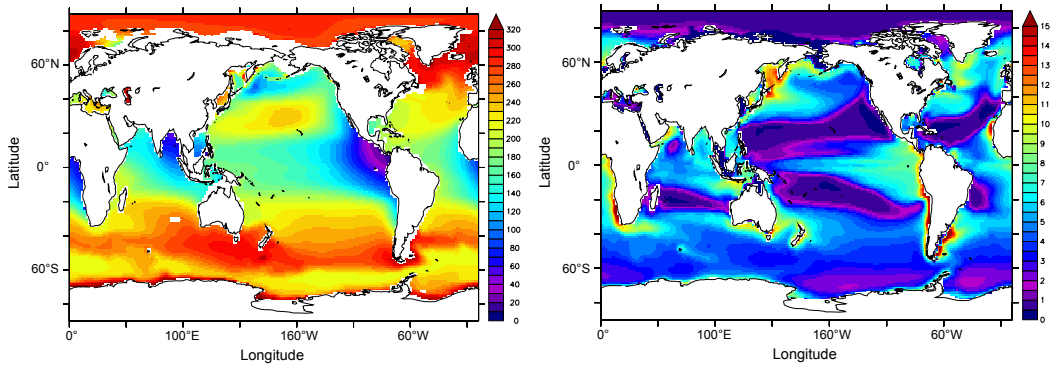

SUPPLEMENTARY MATERIAL

The O_2 modulation fuction $f(O_2)$ in P.OMZ is defined as,

$$f(O_2) = \begin{cases} \dfrac{O_2}{O_2^{*1}} & O_2 < O_2^{*1} \\ 1 & O_2^{*1} < O_2 < O_2^{*2} \\ 0.7 \cdot exp - 0.5(O_2 - O_2^{*2})/O_2^{*2} + & \\ 0.3 \cdot exp - 0.05(O_2 - O_2^{*2})/O_2^{*2} & O_2 \geq O_2^{*2} \end{cases}$$

where O_2^{*1} is 1 µmol L^{-1} and O_2^{*2} is 5 µmol L^{-1}. The shape of the function is shown in Fig. S1.

Fig. S1: Oxygen modulating function $f(O_2)$ in the low-O_2 production pathway term included in P.OMZ from Goreau et al. (1980).

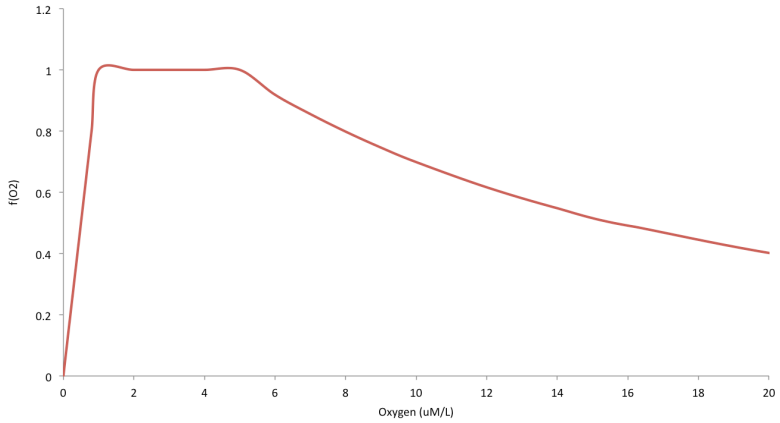

1030 Fig. S2: Vertically integrated (a) high-O_2 and (b) low-O_2 production pathways (in gN m^{-2} yr^{-1})
1031 in P.OMZ for the averaged 1985 to 2005 historical simulation.
1032

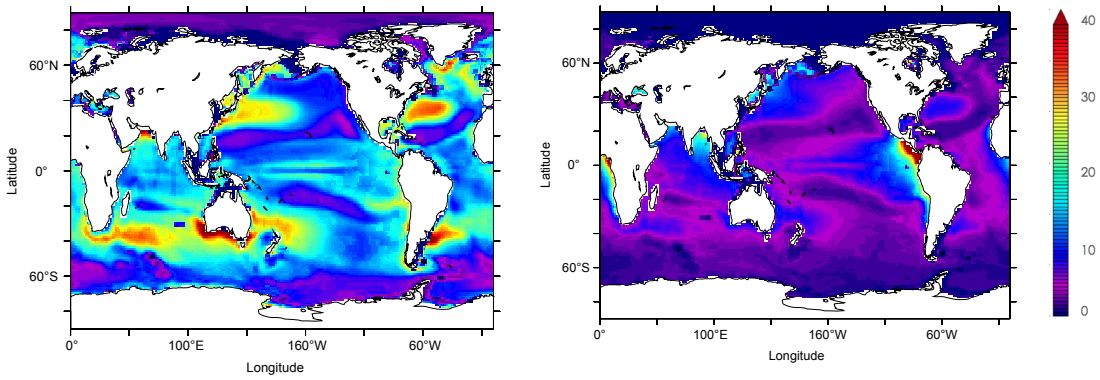

(a) (b)

1033
1034

Fig. S3: Diagram of the box model. N_2O inventory is separated into surface and deep concentrations above and below 100m. The fraction of N_2O outgassed to the atmosphere (*k*), mixing ratio (*v*) between deep and surface and the rate of N_2O production from the export of organic matter to depth (*e*) regulate the N_2O budget in the ocean interior.